

# Interplay between kaon condensation and hyperons in highly dense matter

Takumi Muto\*

Department of Physics, Chiba Institute of Technology, 2-1-1 Shibazono, Narashino, Chiba 275-0023, Japan

(Received 7 February 2007; revised manuscript received 22 November 2007; published 31 January 2008)

The possible coexistence and/or competition of kaon condensation with hyperons are investigated in hyperonic matter, where hyperons are mixed in the ground state of neutron-star matter. The formulation is based on the effective chiral Lagrangian for the kaon-baryon interaction and the nonrelativistic baryon-baryon interaction model. First, the onset condition of the  $s$ -wave kaon condensation realized from hyperonic matter is reexamined. It is shown that the usual assumption of the continuous phase transition is not always kept valid in the presence of the negatively charged hyperons ( $\Sigma^-$ ). Second, the equation of state (EOS) of the kaon-condensed phase in hyperonic matter is discussed. In the case of the stronger kaon-baryon attractive interaction, it is shown that a local energy minimum with respect to the baryon number density appears as a result of considerable softening of the EOS due to both kaon condensation and hyperon mixing and recovering of the stiffness of the EOS at very high densities. This result implies a possible existence of self-bound objects with kaon condensates on any scale from an atomic nucleus to a neutron star.

DOI: 10.1103/PhysRevC.77.015810

PACS number(s): 26.60.-c, 05.30.Jp, 13.75.Jz, 95.35.+d

## I. INTRODUCTION

It has long been suggested that antikaon ( $K^-$ ) condensation should be realized in high-density hadronic matter [1–7].<sup>1</sup> It is characterized as a macroscopic appearance of strangeness in a strongly interacting kaon-baryon system, where chiral symmetry and its spontaneous breaking have key roles. If kaon condensation exists in neutron stars, it softens the hadronic equation of state (EOS), having an influence on the bulk structure of neutron stars such as mass-radius relations [5–8]. Effects of the phase-equilibrium condition associated with the first-order phase transition on the inner structure of neutron stars have also been elucidated [9–14]. With regard to the dynamical evolution of newly born neutron stars, the delayed collapse of protoneutron stars accompanying a phase transition to the kaon-condensed phase has been discussed [15–18]. The existence of kaon condensation is important in the thermal evolution of neutron stars, since the neutrino emission processes are largely enhanced in the presence of kaon condensates [19–22].

In the kaon-condensed phase in neutron stars, the net (negative) strangeness becomes abundant as a consequence of the chemical equilibrium for the weak interaction processes,  $n \rightleftharpoons pK^-$  and  $e^- \rightleftharpoons K^- \nu_e$ . At threshold, the onset condition for kaon condensation has been given as<sup>2</sup>

$$\omega(\rho_B) = \mu, \quad (1)$$

where  $\omega(\rho_B)$  is the lowest  $K^-$  energy obtained at the baryon number density  $\rho_B$  as the zero point of the  $K^-$  inverse propagator  $D_K^{-1}(\omega; \rho_B) = 0$ , and  $\mu$  is the charge chemical potential which is equal to both the antikaon chemical potential  $\mu_K$  and electron chemical potential  $\mu_e$  under the chemical

equilibrium condition for the weak processes [23,24]. This onset condition (1) is based on the assumption of *continuous phase transition*: kaon condensation sets in with zero amplitude at a critical density, above which kaon condensates develop smoothly with increase in baryon number density  $\rho_B$ . It has been shown that the onset condition (1) holds true even if hyperon ( $Y$ ) particle-nucleon ( $N$ ) hole excitation through the  $p$ -wave kaon-baryon interaction is taken into account [25,26] in the ordinary neutron-star matter where only nucleons and leptons are in  $\beta$  equilibrium.

Concerning another hadronic phase including strangeness, hyperons ( $\Lambda$ ,  $\Sigma^-$ ,  $\Xi^-$ , ...) as well as nucleons and leptons have been expected to be mixed in the ground state of neutron-star matter [27–38]. We call the hyperon-mixed neutron-star matter *hyperonic matter* throughout this paper. With regard to coexistence or competition of kaon condensation with hyperons in neutron stars, it has been pointed out that the onset density of the  $s$ -wave kaon condensation subject to condition (1) in hyperonic matter is shifted to a higher density than in the case of the ordinary neutron-star matter [7,28,29]: in hyperonic matter, some of the electrons carrying the negative charge are replaced by the negatively charged hyperons, so the charge chemical potential  $\mu$  [ $= \mu_e = (3\pi^2 \rho_e)^{1/3}$ ] is diminished as compared with that of neutron-star matter without hyperons. As a result, the lowest  $K^-$  energy  $\omega(\rho_B)$  meets the charge chemical potential  $\mu$  at a higher density. Subsequently, several works on the onset density and the EOS for the kaon-condensed phase in hyperonic matter have been elaborated with the relativistic mean-field theory [39,40] or with the quark-meson coupling models [41,42]. Recently the in-medium kaon dynamics and mechanisms of kaon condensation stemming from the  $s$ - and  $p$ -wave kaon-baryon interactions in hyperonic matter have been investigated [43,44].

It is emphasized here that most of the results on the onset mechanisms of kaon condensation in *hyperonic matter* rely on the same assumption as that used in the case of the usual neutron-star matter in which hyperons are not mixed, i.e., the assumption of the *continuous phase transition* with the help of

\*takumi.muto@it-chiba.ac.jp

<sup>1</sup>We consider antikaon ( $K^-$ ) condensation, while we conventionally call it “kaon condensation.”<sup>2</sup>Throughout this paper, the units  $\hbar = c = 1$  are used.

Eq. (1). In this paper, we reexamine the onset condition of kaon condensation realized from hyperonic matter. We consider the  $s$ -wave kaon condensation and incorporate the kaon-baryon interaction within the effective chiral Lagrangian. The nonrelativistic effective baryon-baryon interaction is taken into account, and the parameters are determined so as to reproduce the nuclear saturation properties and baryon potential depths deduced from the recent hypernuclear experiments [45]. We demonstrate that the assumption of continuous phase transition cannot always be applied to the case in which the *negatively charged hyperons* ( $\Sigma^-$ ) are already present in the ground state of hyperonic matter, as a result of competition between the negatively charged kaons and hyperons. It will be shown that in the vicinity of the baryon density a little lower than that at which Eq. (1) is satisfied, another energy solution already exists for which kaons are condensed without mixing of the  $\Sigma^-$  hyperons, in addition to the usual energy solution corresponding to the noncondensed state with  $\Sigma^-$  mixing. In particular, in the case of the stronger kaon-baryon attractive interaction, there is a discontinuous transition between these two states in a small density interval. Thus, from a theoretical viewpoint, one ought to be careful about the previous results concerning coexistence and/or competition of kaon condensates and  $\Sigma^-$  hyperons based on the continuous phase transition, although quantitative effects resulting from the discontinuous phase transition are small.<sup>3</sup>

The interplay between  $K^-$  condensates and  $\Sigma^-$  hyperons can also be revealed in the EOS and characteristic features of the fully developed kaon-condensed phase such as the density dependence of particle fractions. In the case of the stronger kaon-baryon attractive interaction, we will see that a local energy minimum appears with respect to the baryon number density (a density isomer state) as a consequence of considerable softening of the EOS due to both kaon condensation and hyperon mixing and recovering of the stiffness of the EOS at very high densities due to the increase in the repulsive interaction between baryons.

The paper is organized as follows. In Sec. II, the formulation to obtain the effective energy density of the kaon-condensed phase in hyperonic matter is presented. In Sec. III, numerical results for the composition of the noncondensed phase of hyperonic matter are given for the sake of the subsequent discussions. Section IV is devoted to the discussion of the validity of the continuous phase transition. The results for the EOS of the kaon-condensed phase are given in Sec. V. In Sec. VI, summary and concluding remarks are addressed. In the Appendix, we remark that the two sets of parameters used in this paper for the baryon-baryon interaction models give different behaviors for the onset of  $\Lambda$  and  $\Sigma^-$  hyperons in ordinary neutron-star matter.

## II. FORMULATION

### A. Outline of the kaon-condensed matter

To simplify and clarify the discussion about the interrelations between kaon condensation and hyperons, we consider the  $s$ -wave kaon condensation by putting the kaon momentum  $|\mathbf{k}| = 0$ , and we also take into account only the proton ( $p$ ),  $\Lambda$ , neutron ( $n$ ), and  $\Sigma^-$  of the octet baryons and the ultrarelativistic electrons for kaon-condensed hyperonic matter in neutron stars.<sup>4</sup>

Within chiral symmetry, the classical kaon field as an order parameter of the  $s$ -wave kaon condensation is chosen to be a spatially uniform type:

$$\langle K^- \rangle = \frac{f}{\sqrt{2}} \theta e^{-i\mu_K t}, \quad (2)$$

where  $\theta$  is the chiral angle as an amplitude of condensation, and  $f$  ( $\sim f_\pi = 93$  MeV) is the meson decay constant.

We impose the charge neutrality condition and baryon number conservation, and we construct the effective Hamiltonian density by introducing the charge chemical potential  $\mu$  and the baryon number chemical potential  $\nu$ , respectively, as the Lagrange multipliers corresponding to these two conditions. The resulting effective energy density is then written in the form

$$\mathcal{E}_{\text{eff}} = \mathcal{E} + \mu(\rho_p - \rho_{\Sigma^-} - \rho_{K^-} - \rho_e) + \nu(\rho_p + \rho_\Lambda + \rho_n + \rho_{\Sigma^-}), \quad (3)$$

where  $\mathcal{E}$  is the total energy density of the kaon-condensed phase, and  $\rho_i$  ( $i = p, \Lambda, n, \Sigma^-, K^-, e^-$ ) are the number densities of the particles  $i$ . Note that the number density of the kaon condensates  $\rho_{K^-}$  consists of the free kaon part and the kaon-baryon interaction part of the vector type [see Eq. (18)]. From the extremum conditions for  $\mathcal{E}_{\text{eff}}$  with respect to the variation of  $\rho_i$ , one obtains the relations

$$\mu_K = \mu_e = \mu_n - \mu_p = \mu_{\Sigma^-} - \mu_n = \mu, \quad (4a)$$

$$\mu_\Lambda = \mu_n = -\nu, \quad (4b)$$

where  $\mu_i$  ( $i = p, \Lambda, n, \Sigma^-, K^-, e^-$ ) are the chemical potentials, which are given by  $\mu_i = \partial \mathcal{E} / \partial \rho_i$ . Equations (4a) and (4b) imply that the system is in chemical equilibrium for the weak interaction processes,  $n \rightleftharpoons pK^-$ ,  $n \rightleftharpoons pe^-(\bar{\nu}_e)$ ,  $ne^- \rightleftharpoons \Sigma^-(\nu_e)$ , and  $n \rightleftharpoons \Lambda(\nu_e \bar{\nu}_e)$ .

### B. Kaon-baryon interaction

We base our study of the kaon-baryon interaction on chiral symmetry and start with the effective chiral  $SU(3)_L \times SU(3)_R$

<sup>3</sup>Our discussion is concentrated on obtaining the energy solutions in the presence of hyperons under the constraints relevant to neutron stars. We do not discuss here the prescription of the Gibbs condition for the phase equilibrium associated with a first-order phase transition [9–14]. This issue will be reported elsewhere [46]. A first-order phase transition to the  $K^-$ -condensed phase has also been discussed in another context in Refs. [26,44].

<sup>4</sup>Note that the other hyperons may also appear over the relevant densities in neutron stars. In particular, the  $\Xi^-$  hyperons may begin to be mixed at a lower density than the  $\Sigma^-$  hyperons in the case of the repulsive potential for the  $\Sigma^-$  in nuclear matter [28,29,36,43]. In this paper, we just neglect the  $\Xi^-$  for simplicity and consider only the  $\Sigma^-$  as a negatively charged hyperon.

Lagrangian [1].<sup>5</sup> Then the relevant Lagrangian density, leading to the total energy density  $\mathcal{E}$ , consists of the following parts:

$$\begin{aligned}\mathcal{L} = & \frac{1}{4}f^2\text{Tr}\partial^\mu\Sigma^\dagger\partial_\mu\Sigma + \frac{1}{2}f^2\Lambda_{\chi\text{SB}}(\text{Tr}M(\Sigma - 1) + \text{h.c.}) \\ & + \text{Tr}\bar{\Psi}(i\not{\partial} - M_B)\Psi + \text{Tr}\bar{\Psi}i\not{\gamma}^\mu[V_\mu, \Psi] \\ & + a_1\text{Tr}\bar{\Psi}(\xi M^\dagger\xi + \text{h.c.})\Psi + a_2\text{Tr}\bar{\Psi}\Psi(\xi M^\dagger\xi + \text{h.c.}) \\ & + a_3(\text{Tr}M\Sigma + \text{h.c.})\text{Tr}\bar{\Psi}\Psi,\end{aligned}\quad (5)$$

where the first and second terms on the right-hand side of Eq. (5) are the kinetic and mass terms of mesons, respectively.  $\Sigma$  is the nonlinear meson field defined by  $\Sigma \equiv e^{2i\Pi/f}$ , where  $\Pi \equiv \sum_{a=1\sim 8}\pi_a T_a$  with  $\pi_a$  being the octet meson fields and  $T_a$  being the SU(3) generators. Since only charged kaon condensation is considered, the  $\Pi$  is simply written as

$$\Pi = \frac{1}{\sqrt{2}} \begin{pmatrix} 0 & 0 & K^+ \\ 0 & 0 & 0 \\ K^- & 0 & 0 \end{pmatrix}. \quad (6)$$

In the second term on the right-hand side of Eq. (5),  $\Lambda_{\chi\text{SB}}$  is the chiral symmetry breaking scale,  $\sim 1$  GeV, and  $M$  is the mass matrix given by  $M \equiv \text{diag}(m_u, m_d, m_s)$  with the quark masses  $m_i$ . The third term in Eq. (5) denotes the free baryon part, where  $\Psi$  is the octet baryon field including only the  $p, \Lambda, n$ , and  $\Sigma^-$ ; and  $M_B$  is the baryon mass generated as a consequence of spontaneous chiral symmetry breaking. The fourth term in Eq. (5) gives the  $s$ -wave kaon-baryon interaction of the vector type corresponding to the Tomozawa-Weinberg term with  $V_\mu$  being the mesonic vector current defined by  $V_\mu \equiv 1/2(\xi^\dagger\partial_\mu\xi + \xi\partial_\mu\xi^\dagger)$  with  $\xi \equiv \Sigma^{1/2}$ . The last three terms in Eq. (5) give the  $s$ -wave meson-baryon interaction of the scalar type, which explicitly breaks chiral symmetry.<sup>6</sup>

The quark masses  $m_i$  are chosen to be  $m_u = 6$  MeV,  $m_d = 12$  MeV, and  $m_s = 240$  MeV. Together with these values, the parameters  $a_1$  and  $a_2$  are fixed to be  $a_1 = -0.28$  and  $a_2 = 0.56$  so as to reproduce the empirical octet baryon mass splittings [1]. The parameter  $a_3$  is related to the kaon-nucleon ( $KN$ ) sigma terms simulating the  $s$ -wave  $KN$  attraction of the scalar type through the expressions  $\Sigma_{Kp} = -(a_1 + a_2 + 2a_3)(m_u + m_s)$ ,  $\Sigma_{Kn} = -(a_2 + 2a_3)(m_u + m_s)$ , evaluated at the on-shell Cheng-Dashen point for the effective chiral Lagrangian (5). Recent lattice calculations suggest the value of the  $KN$  sigma term  $\Sigma_{Kn} = 300\text{--}400$  MeV [48]. We take the value of  $a_3 = -0.9$ , leading to  $\Sigma_{Kn} = 305$  MeV, as a standard value. For comparison, we also take another value  $a_3 = -0.7$ , which leads to  $\Sigma_{Kn} = 207$  MeV. The  $K^-$  optical potential in symmetric nuclear matter,  $V_{\text{opt}}(\rho_B)$ , is estimated as a scale of the  $K^-$ -nucleon attractive interaction. It is defined by

$$V_{\text{opt}}(\rho_B) = \Pi_{K^-}(\omega(\rho_B), \rho_B)/2\omega(\rho_B), \quad (7)$$

where  $\Pi_{K^-}(\omega(\rho_B), \rho_B)$  is the  $K^-$  self-energy at given  $\rho_B$  with  $\rho_p = \rho_n = \rho_B/2$ . For  $a_3 = -0.9$  ( $a_3 = -0.7$ ),  $V_{\text{opt}}(\rho_0)$

is estimated to be  $-115$  MeV ( $-95$  MeV) at the nuclear saturation density  $\rho_0 (= 0.16 \text{ fm}^{-3})$ .

To be consistent with the on-shell  $s$ -wave  $K(\bar{K})$ - $N$  scattering lengths, we have to take into account the range terms proportional to  $\omega^2$  coming from the higher-order terms in chiral expansion and a pole contribution from the  $\Lambda(1405)$ . Nevertheless, these contributions to the energy density become negligible in high-density matter as far as  $K^-$  condensation is concerned [4,5]. Therefore, we omit these correction terms throughout this paper and consider the simplified expression for the energy density of the kaon-condensed phase.

### C. Effective energy density

The total effective energy density  $\mathcal{E}_{\text{eff}}$  is separated into baryon, meson, and lepton parts as  $\mathcal{E}_{\text{eff}} = \mathcal{E}_{\text{eff}}^B + \mathcal{E}_{\text{eff}}^M + \mathcal{E}_{\text{eff}}^e$ . The kaon-baryon interaction is incorporated in the baryon part  $\mathcal{E}_{\text{eff}}^B$ , and the meson part  $\mathcal{E}_{\text{eff}}^M$  consists of the free classical kaons only. The baryon part  $\mathcal{E}_{\text{eff}}^B$  and the meson part  $\mathcal{E}_{\text{eff}}^M$  are derived from the effective chiral Lagrangian (5). After the nonrelativistic reduction for the baryon part of the effective Hamiltonian by way of the Foldy-Wouthuysen-Tani transformation and with the mean-field approximation, one obtains

$$\mathcal{E}_{\text{eff}}^B = \sum_{i=p,\Lambda,n,\Sigma^-} \sum_{|\mathbf{p}| \leq |\mathbf{p}_F(i)|} \sum_{s=\pm 1/2} E_{\text{eff},s}^{(i)}(\mathbf{p}), \quad (8)$$

where  $\mathbf{p}_F(i)$  are the Fermi momenta, and the subscript  $s$  stands for the spin states for the baryon. The effective single-particle energies  $E_{\text{eff},s}^{(i)}(\mathbf{p})$  for the baryons  $i$  are represented by

$$E_{\text{eff},s}^{(p)}(\mathbf{p}) = \mathbf{p}^2/2M_N - (\mu + \Sigma_{Kp})(1 - \cos\theta) + \mu + \nu, \quad (9a)$$

$$E_{\text{eff},s}^{(\Lambda)}(\mathbf{p}) = \mathbf{p}^2/2M_N - \Sigma_{K\Lambda}(1 - \cos\theta) + \delta M_{\Lambda N} + \nu, \quad (9b)$$

$$E_{\text{eff},s}^{(n)}(\mathbf{p}) = \mathbf{p}^2/2M_N - (\frac{1}{2}\mu + \Sigma_{Kn})(1 - \cos\theta) + \nu, \quad (9c)$$

$$\begin{aligned}E_{\text{eff},s}^{(\Sigma^-)}(\mathbf{p}) = & \mathbf{p}^2/2M_N - (\frac{1}{2}\mu + \Sigma_{K\Sigma^-})(1 - \cos\theta) \\ & + \delta M_{\Sigma^- N} - \mu + \nu,\end{aligned} \quad (9d)$$

where  $M_N$  is the nucleon mass,  $\delta M_{\Lambda N} (= 176 \text{ MeV})$  is the  $\Lambda$ - $N$  mass difference and  $\delta M_{\Sigma^- N} (= 258 \text{ MeV})$  the  $\Sigma^-$ - $N$  mass difference. The “kaon-hyperon sigma terms” are defined by  $\Sigma_{K\Lambda} \equiv -(\frac{5}{6}a_1 + \frac{5}{6}a_2 + 2a_3)(m_u + m_s)$  and  $\Sigma_{K\Sigma^-} \equiv -(a_2 + 2a_3)(m_u + m_s) (= \Sigma_{Kn})$ . Note that each term in Eqs. (9) contains both the kaon-baryon attraction of the scalar type simulated by the sigma term and the kaon-baryon interaction of the vector type proportional to  $\mu$ , the coefficient of which is given by the V-spin charge of each baryon.

The meson contribution to the effective energy density  $\mathcal{E}_{\text{eff}}^M$  is given by the substitution of the classical kaon field [Eq. (2)] into the meson part of the effective Hamiltonian, that is,

$$\mathcal{E}_{\text{eff}}^M = -\frac{1}{2}f^2\mu^2\sin^2\theta + f^2m_K^2(1 - \cos\theta), \quad (10)$$

where  $m_K \equiv [\Lambda_{\chi\text{SB}}(m_u + m_s)]^{1/2}$ , which is identified with the free kaon mass, and is replaced by the experimental value  $493.7$  MeV. The lepton contribution to the effective energy

<sup>5</sup>Except for setting  $|\mathbf{k}| = 0$ , the basic formulation presented here is the same as that in Ref. [43], where both  $s$ -wave and  $p$ -wave kaon-baryon interactions are incorporated.

<sup>6</sup>The same types of scalar and vector interactions are derived in the quark-meson coupling model [47].

density is given as

$$\mathcal{E}_{\text{eff}}^e = \frac{\mu^4}{4\pi^2} - \mu \frac{\mu^3}{3\pi^2} = -\frac{\mu^4}{12\pi^2}, \quad (11)$$

with  $\rho_e = \mu^3/(3\pi^2)$  for the ultrarelativistic electrons.

#### D. Baryon potentials

We introduce a potential energy density  $\mathcal{E}_{\text{pot}}$  as a local effective baryon-baryon interaction, which is assumed to be given by functions of the number densities of the relevant baryons [36]. To consistently take into account the baryon potential effects on both the whole energy of the system and the baryon single-particle energies, we take the following prescription: the baryon potential  $V_i (i = p, \Lambda, n, \Sigma^-)$  is defined as

$$V_i = \partial \mathcal{E}_{\text{pot}} / \partial \rho_i, \quad (12)$$

with  $\rho_i$  being the number density of baryon  $i$ , and it is added to each effective single particle energy,  $E_{\text{eff},s}^{(i)}(\mathbf{p}) \rightarrow E_{\text{eff},s}^{\prime(i)}(\mathbf{p}) = E_{\text{eff},s}^{(i)}(\mathbf{p}) + V_i$ . The potential energy density  $\mathcal{E}_{\text{pot}}$  is added to the total effective energy density  $\mathcal{E}^{\text{eff}}$ , and the term  $\sum_{i=p,\Lambda,n,\Sigma^-} \rho_i V_i$  is subtracted to avoid the double counting of the baryon interaction energies in the sum over the effective single-particle energies  $E_{\text{eff},s}^{\prime(i)}(\mathbf{p})$ . Accordingly, the baryon part of the effective energy density is modified as

$$\begin{aligned} \mathcal{E}_{\text{eff}}^{\prime B} &= \sum_{i=p,\Lambda,n,\Sigma^-} \sum_{\substack{|\mathbf{p}| \leq |\mathbf{p}_F^{(i)}| \\ s=\pm 1/2}} E_{\text{eff},s}^{\prime(i)}(\mathbf{p}) + \mathcal{E}_{\text{pot}} - \sum_{i=p,\Lambda,n,\Sigma^-} \rho_i V_i \\ &= \frac{3}{5} \frac{(3\pi^2)^{2/3}}{2M_N} (\rho_p^{5/3} + \rho_\Lambda^{5/3} + \rho_n^{5/3} + \rho_{\Sigma^-}^{5/3}) \\ &\quad + (\rho_\Lambda \delta M_{\Lambda p} + \rho_{\Sigma^-} \delta M_{\Sigma^- n}) + \mathcal{E}_{\text{pot}} \\ &\quad - \left\{ \rho_p (\mu + \Sigma_{Kp}) + \rho_\Lambda \Sigma_{K\Lambda} + \rho_n \left( \frac{1}{2} \mu + \Sigma_{Kn} \right) \right. \\ &\quad \left. + \rho_{\Sigma^-} \left( -\frac{1}{2} \mu + \Sigma_{K\Sigma^-} \right) \right\} (1 - \cos \theta) \\ &\quad + \mu (\rho_p - \rho_{\Sigma^-}) + \nu \rho_B. \end{aligned} \quad (13)$$

The total effective energy density  $\mathcal{E}'_{\text{eff}}$  is obtained as the sum of the baryon, meson, and lepton parts whose explicit forms are given by Eqs. (13), (10), and (11), respectively. For later convenience, we also show the total energy density  $\mathcal{E}'$  including the potential contribution for baryons as

$$\begin{aligned} \mathcal{E}' &= \frac{3}{5} \frac{(3\pi^2)^{2/3}}{2M_N} (\rho_p^{5/3} + \rho_\Lambda^{5/3} + \rho_n^{5/3} + \rho_{\Sigma^-}^{5/3}) \\ &\quad + (\rho_\Lambda \delta M_{\Lambda N} + \rho_{\Sigma^-} \delta M_{\Sigma^- N}) + \mathcal{E}_{\text{pot}} \\ &\quad - (\rho_p \Sigma_{Kp} + \rho_\Lambda \Sigma_{K\Lambda} + \rho_n \Sigma_{Kn} + \rho_{\Sigma^-} \Sigma_{K\Sigma^-}) (1 - \cos \theta) \\ &\quad + \frac{1}{2} f^2 \mu^2 \sin^2 \theta + f^2 m_K^2 (1 - \cos \theta) + \mu^4 / (4\pi^2), \end{aligned} \quad (14)$$

where the first term on the right-hand side denotes the baryon kinetic energy, the second term comes from the mass difference between the hyperons and nucleons, the third term is the baryon potential energy, the fourth term is the  $s$ -wave kaon-baryon scalar interaction brought about by the kaon-baryon sigma

terms, the fifth and sixth terms are the free parts of the condensed kaon energy (kinetic energy and free mass), and the last term stands for the lepton kinetic energy.

For the hyperonic matter composed of  $p$ ,  $\Lambda$ ,  $n$ , and  $\Sigma^-$ , the potential energy density  $\mathcal{E}_{\text{pot}}$  is given by

$$\begin{aligned} \mathcal{E}_{\text{pot}} &= \frac{1}{2} [a_{NN}(\rho_p + \rho_n)^2 + b_{NN}(\rho_p - \rho_n)^2 \\ &\quad + c_{NN}(\rho_p + \rho_n)^{\delta+1}] + a_{\Lambda N}(\rho_p + \rho_n)\rho_\Lambda \\ &\quad + c_{\Lambda N} \left[ \frac{(\rho_p + \rho_n)^{\gamma+1}}{\rho_p + \rho_n + \rho_\Lambda} \rho_\Lambda + \frac{\rho_\Lambda^{\gamma+1}}{\rho_p + \rho_n + \rho_\Lambda} (\rho_p + \rho_n) \right] \\ &\quad + \frac{1}{2} (a_{YY}\rho_\Lambda^2 + c_{YY}\rho_\Lambda^{\gamma+1}) + a_{\Sigma N}(\rho_p + \rho_n)\rho_{\Sigma^-} \\ &\quad + b_{\Sigma N}(\rho_n - \rho_p)\rho_{\Sigma^-} \\ &\quad + c_{\Sigma N} \left[ \frac{(\rho_p + \rho_n)^{\gamma+1}}{\rho_p + \rho_n + \rho_{\Sigma^-}} \rho_{\Sigma^-} + \frac{\rho_{\Sigma^-}^{\gamma+1}}{\rho_p + \rho_n + \rho_{\Sigma^-}} (\rho_p + \rho_n) \right] \\ &\quad + a_{YY}\rho_{\Sigma^-}\rho_\Lambda + c_{YY} \left[ \frac{\rho_{\Sigma^-}^{\gamma+1}}{\rho_{\Sigma^-} + \rho_\Lambda} \rho_\Lambda + \frac{\rho_\Lambda^{\gamma+1}}{\rho_{\Sigma^-} + \rho_\Lambda} \rho_{\Sigma^-} \right] \\ &\quad + \frac{1}{2} [(a_{YY} + b_{\Sigma\Sigma})\rho_{\Sigma^-}^2 + c_{YY}\rho_{\Sigma^-}^{\gamma+1}], \end{aligned} \quad (15)$$

where the terms including the exponents  $\delta$  and  $\gamma$  ( $\delta, \gamma > 1$ ) represent the multibody repulsive interactions between baryons. The parameters in the potential energy density of Eq. (15) are determined as follows. (i) The parameters  $a_{NN}$  and  $c_{NN}$  in the  $NN$  part are fixed so as to reproduce the standard nuclear saturation density  $\rho_0 = 0.16 \text{ fm}^{-3}$  and the binding energy  $-16 \text{ MeV}$  in symmetric nuclear matter. With the parameters  $a_{NN}$ ,  $c_{NN}$ , and  $\delta$ , the incompressibility  $K$  in symmetric nuclear matter is obtained. The parameter  $b_{NN}$  for the isospin-dependent term in the  $NN$  part is chosen to reproduce the empirical value of the symmetry energy  $\sim 30 \text{ MeV}$  at  $\rho_B = \rho_0$ . (ii) For the  $YN$  parts,  $a_{\Lambda N}$  and  $c_{\Lambda N}$  are basically taken to be the same as those in Ref. [36], where the single  $\Lambda$  orbitals in ordinary hypernuclei are reasonably fitted. The depth of the  $\Lambda$  potential in nuclear matter is then given as  $V_\Lambda(\rho_p = \rho_n = \rho_0/2) = a_{\Lambda N}\rho_0 + c_{\Lambda N}\rho_0^\gamma = -27 \text{ MeV}$  [49]. The depth of the  $\Sigma^-$  potential  $V_{\Sigma^-}$  in nuclear matter is taken to be repulsive, following recent theoretical calculations [50,51] and the phenomenological analyses on the  $(K^-, \pi^\pm)$  reactions at BNL [52,53],  $(\pi^-, K^+)$  reactions at KEK [54–56], and the  $\Sigma^-$  atom data [57]:  $V_{\Sigma^-}(\rho_p = \rho_n = \rho_0/2) = a_{\Sigma N}\rho_0 + c_{\Sigma N}\rho_0^\gamma = 23.5 \text{ MeV}$  and  $b_{\Sigma N}\rho_0 = 40.2 \text{ MeV}$ . This choice of the parameters corresponds to the values in Ref. [53] based on the Nijmegen model F. (iii) Since the experimental information on the  $YY$  interactions is not enough, we take the same parameters for the  $YY$  part as those in Ref. [36].

Taking into account the conditions (i)–(iii), we adopt the following two parameter sets throughout this paper. (A)  $\delta = \gamma = 5/3$ . In this case, one obtains  $K = 306 \text{ MeV}$ , which is larger than the standard empirical value  $210 \pm 30 \text{ MeV}$  [58]. (B)  $\delta = 4/3$  and  $\gamma = 2.0$ . From the choice  $\delta = 4/3$ , one obtains  $K = 236 \text{ MeV}$ , which lies within the empirical value. The choice  $\gamma = 2.0$  leads to the stiffer EOS for hyperonic matter



TABLE I. Parameters in the potential energy density.

H-EOS	Parameter	Parameter	Parameter
(A)	$\gamma$	5/3	$a_{\Lambda N}^a$ -387.0
	$\delta$	5/3	$c_{\Lambda N}^b$ 738.8
	$a_{NN}^a$	-914.2	$a_{\Sigma N}^a$ -70.9
	$b_{NN}^a$	212.8	$b_{\Sigma N}^a$ 251.3
	$c_{NN}^c$	1486.4	$c_{\Sigma N}^b$ 738.8
(B)	$\gamma$	2	$a_{\Lambda N}^a$ -342.8
	$\delta$	4/3	$c_{\Lambda N}^b$ 1087.5
	$a_{NN}^a$	-1352.3	$a_{\Sigma N}^a$ -27.1
	$b_{NN}^a$	212.8	$b_{\Sigma N}^a$ 251.3
	$c_{NN}^c$	1613.9	$c_{\Sigma N}^b$ 1087.5

<sup>a</sup>MeV fm<sup>3</sup>.<sup>b</sup>MeV fm<sup>3</sup> $\gamma$ .<sup>c</sup>MeV fm<sup>3</sup> $\delta$ .

at high densities compared with case (A). Numerical values of the parameter sets (A) and (B) are listed in Table I. Here we abbreviate the EOS for hyperonic matter with the use of (A) and (B) as H-EOS (A) and H-EOS (B), respectively.

### E. Physical constraints

The energy density and physical quantities in the ground state are obtained variationally by the extremization of the total effective energy density  $\mathcal{E}'_{\text{eff}}$  with respect to  $\theta$ ,  $\mu$ , and each number density of the baryon  $i$  at a given density  $\rho_B$ . From  $\partial\mathcal{E}'_{\text{eff}}/\partial\theta = 0$ , one obtains the classical field equation for  $\theta$ ,

$$\sin\theta \left[ \mu^2 \cos\theta - m_K^2 + \frac{\mu}{f^2} \left( \rho_p + \frac{1}{2}\rho_n - \frac{1}{2}\rho_{\Sigma^-} \right) + \frac{1}{f^2} \sum_{i=p,\Lambda,n,\Sigma^-} \rho_i \Sigma_{Ki} \right] = 0. \quad (16)$$

From  $\partial\mathcal{E}'_{\text{eff}}/\partial\mu = 0$ , one obtains the charge neutrality condition

$$\rho_p - \rho_{\Sigma^-} - \rho_{K^-} - \rho_e = 0, \quad (17)$$

where the number density of the kaon condensates  $\rho_{K^-}$  is given as

$$\rho_{K^-} = \mu f^2 \sin^2\theta + \left( \rho_p + \frac{1}{2}\rho_n - \frac{1}{2}\rho_{\Sigma^-} \right) (1 - \cos\theta). \quad (18)$$

From  $\partial\mathcal{E}'_{\text{eff}}/\partial v = \rho_B$ , one obtains the baryon number conservation

$$\sum_{i=p,\Lambda,n,\Sigma^-} \rho_i = \rho_B. \quad (19)$$

The chemical equilibrium conditions for the weak interaction processes [Eq. (4)],  $n \rightleftharpoons pe^-(\bar{\nu}_e)$ ,  $n \rightleftharpoons \Lambda(\nu_e \bar{\nu}_e)$ , and  $ne^- \rightleftharpoons \Sigma^-(\nu_e)$ , are rewritten as

$$\mu_n = \mu_p + \mu, \quad (20a)$$

$$\mu_\Lambda = \mu_n, \quad (20b)$$

$$\mu_{\Sigma^-} = \mu_n + \mu, \quad (20c)$$

where the chemical potentials for the baryons are given by  $\mu_i = \partial\mathcal{E}'/\partial\rho_i$  with the help of Eqs. (14), (16), and (18); that is,

$$\mu_n = \frac{(3\pi^2\rho_n)^{2/3}}{2M_N} - \left( \frac{1}{2}\mu + \Sigma_{Kn} \right) (1 - \cos\theta) + V_n, \quad (21a)$$

$$\mu_p = \frac{(3\pi^2\rho_p)^{2/3}}{2M_N} - (\mu + \Sigma_{Kp})(1 - \cos\theta) + V_p, \quad (21b)$$

$$\mu_\Lambda = \frac{(3\pi^2\rho_\Lambda)^{2/3}}{2M_N} - \Sigma_{K\Lambda}(1 - \cos\theta) + \delta M_{\Lambda N} + V_\Lambda, \quad (21c)$$

$$\mu_{\Sigma^-} = \frac{(3\pi^2\rho_{\Sigma^-})^{2/3}}{2M_N} - \left( -\frac{1}{2}\mu + \Sigma_{K\Sigma^-} \right) (1 - \cos\theta) + \delta M_{\Sigma^- N} + V_{\Sigma^-}. \quad (21d)$$

### III. COMPOSITION OF MATTER IN THE NONCONDENSED PHASE

The critical density satisfying Eq. (1) depends sensitively on the density dependence of  $\mu$ , which is also affected by the matter composition through the relation  $\mu = \mu_e = (3\pi^2\rho_e)^{1/3}$ .

Thereby, before going into detail on the onset density of kaon condensation, we address behaviors of particle fractions in the noncondensed hyperonic matter.

In Figs. 1 and 2, particle fractions  $\rho_i/\rho_B$  ( $i = p, \Lambda, n, \Sigma^-, e^-$ ) in the noncondensed hyperonic matter are shown as functions of baryon number density  $\rho_B$  for H-EOS (A) and (B), respectively. In both figures, the dashed lines stand for the ratio of the total negative strangeness number density  $\rho_{\text{strange}} (= \rho_\Lambda + \rho_{\Sigma^-})$  to the baryon number density  $\rho_B$ .

In the case of H-EOS (A), the  $\Lambda$  hyperon starts to be mixed at  $\rho_B = \rho_B^c(\Lambda) = 0.340 \text{ fm}^{-3} (= 2.13\rho_0)$  and the  $\Sigma^-$  hyperon does the same at a higher density,  $\rho_B = \rho_B^c(\Sigma^-) = 0.525 \text{ fm}^{-3} (= 3.28\rho_0)$  (Fig. 1). For H-EOS (B), both hyperons start to be mixed at higher densities than the case of H-EOS (A), i.e., at  $\rho_B = \rho_B^c(\Lambda) \sim 0.44 \text{ fm}^{-3} (= 2.69\rho_0)$  for the  $\Lambda$  and

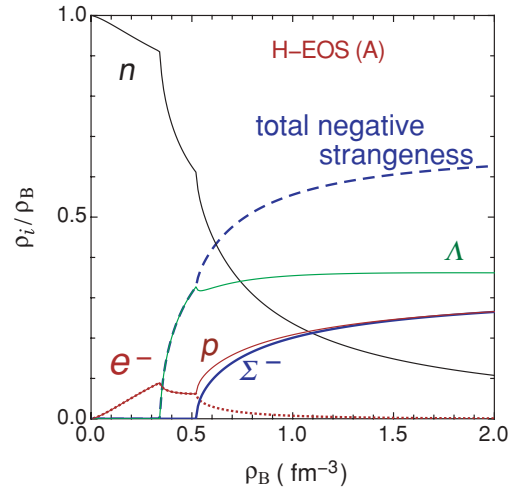


FIG. 1. (Color online) Particle fractions  $\rho_i/\rho_B$  in the noncondensed hyperonic matter as functions of baryon number density  $\rho_B$ . The H-EOS (A) is used.

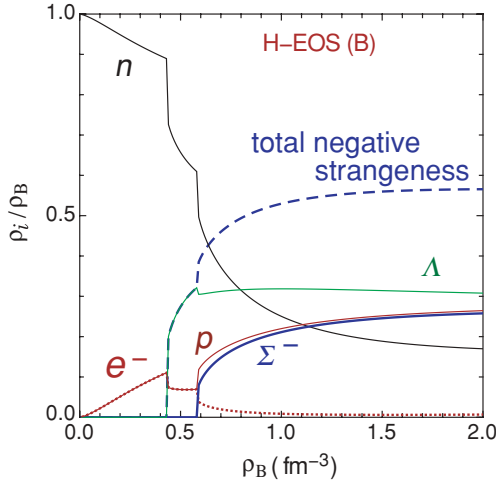


FIG. 2. (Color online) Same as in Fig. 1, but for H-EOS (B).

$\rho_B = \rho_B^c(\Sigma^-) \sim 0.59 \text{ fm}^{-3} (=3.69\rho_0)$  for the  $\Sigma^-$  (Fig. 2). In fact, the condition for  $\Lambda$  mixing in the  $(n, p, e^-)$  matter, for instance, is written by the use of Eqs. (21a) and (21c) as

$$\delta M_{\Lambda N} + V_{\Lambda} \leq \frac{(3\pi^2 \rho_n)^{2/3}}{2M_N} + V_n, \quad (22)$$

where  $V_{\Lambda} = a_{\Lambda N} \rho_B + c_{\Lambda N} \rho_B^{\gamma}$  and  $V_n = a_{NN} \rho_B - b_{NN}(\rho_p - \rho_n) + \frac{1}{2} c_{NN}(\delta + 1) \rho_B^{\delta}$ . In the case of H-EOS (B), the exponent  $\delta (=4/3)$  is smaller than that for H-EOS (A) ( $=5/3$ ), which makes the repulsive interaction of  $V_n$  for H-EOS (B) smaller than that for H-EOS (A). Furthermore the exponent  $\gamma (=2)$  is bigger than that for H-EOS (A) ( $=5/3$ ), which makes the repulsive interaction of  $V_{\Lambda}$  for H-EOS (B) larger than that for H-EOS (A). Both effects push up the threshold density for the condition (22) as compared with the case of H-EOS (A).

In general, the smaller value of the exponent  $\delta$  simulating the higher-order terms of the repulsive nucleon-nucleon interactions gives the smaller potential energy contributions for the nucleons. The larger value of the exponent  $\gamma$  simulating the higher-order repulsive terms of the hyperon-nucleon and hyperon-hyperon interactions gives the larger potential energy contributions for the hyperons. As a result, the  $\beta$  equilibrium conditions for the hyperons,  $n \rightleftharpoons \Lambda(\nu_e \bar{\nu}_e)$  and  $ne^- \rightleftharpoons \Sigma^-(\nu_e)$ , are satisfied at higher densities for H-EOS (B) than for H-EOS (A).

Note that for H-EOS (B), the  $\Lambda$  and  $\Sigma^-$  start to appear in the ground state of neutron-star matter such that the mixing ratios  $\rho_{\Lambda}/\rho_B$  and  $\rho_{\Sigma^-}/\rho_B$  increase discontinuously from zero to finite nonzero values above certain densities. This is a different behavior from the usual one, where the hyperon-mixing ratios increase continuously from zero as density increases, as in the case of H-EOS (A). (See the Appendix.)

One can see common behavior with regard to the density dependence of each particle fraction for H-EOS (A) and (B): as the hyperons dominate the matter composition with increase in  $\rho_B$ , the electron fraction decreases. In particular, the negative charge of the electron is taken over by that of the  $\Sigma^-$  hyperon, so that the electron fraction decreases rapidly, while the  $\Sigma^-$  fraction increases as the density increases. The proton fraction

increases so as to compensate the negative charge of the  $\Sigma^-$ . At high densities, the  $\Sigma^-$  and proton fractions amount to 20–30%, the  $\Lambda$  fraction to 30–40%, and the fraction of total negative strangeness to 50–60%. As a result of the increases in the proton,  $\Lambda$ , and  $\Sigma^-$  fractions, the neutron fraction decreases rapidly with increase in  $\rho_B$ .

#### IV. VALIDITY OF CONTINUOUS PHASE TRANSITION

In ordinary neutron-star matter without hyperon mixing, the onset density for kaon condensation is given by the condition  $\omega = \mu$  [Eq. (1)]. Here the lowest energy  $\omega$  for  $K^-$  is obtained from the zero point of the inverse propagator for  $K^-$ ,  $D_K^{-1}(\omega; \rho_B)$ , which can be read from the expansion of the total effective energy density  $\mathcal{E}'_{\text{eff}}$  with respect to the chiral angle  $\theta$  around  $\theta = 0$ :

$$\mathcal{E}'_{\text{eff}}(\theta) = \mathcal{E}'_{\text{eff}}(0) - \frac{f^2}{2} D_K^{-1}(\mu; \rho_B) \theta^2 + O(\theta^4). \quad (23)$$

This onset condition,  $D_K^{-1}(\mu; \rho_B) = 0$ , is equal to the non-trivial classical kaon-field equation (16) with  $\theta = 0$  and is based on the assumption of the continuous phase transition: the chiral angle  $\theta$ , for instance, increases continuously from zero as  $\rho_B$  increases. In this section, we consider the validity of the assumption of the continuous phase transition to  $K^-$  condensation in hyperonic matter. Numerical results are presented by the use of H-EOS (A) and (B) for the noncondensed hyperonic matter EOS in Secs. IV A and IV B, respectively.

##### A. Case of H-EOS (A)

In Fig. 3, we show the lowest energies of  $K^-$  as functions of baryon number density  $\rho_B$  for  $\Sigma_{Kn} = 305$  and 207 MeV in the case of H-EOS (A). The dependence of the charge chemical potential  $\mu (= \mu_K = \mu_e)$  on  $\rho_B$  is shown by the dotted line. The charge chemical potential  $\mu$  decreases with increase in density

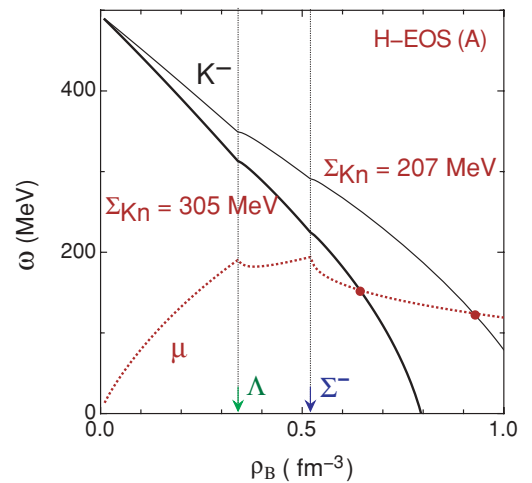


FIG. 3. (Color online) Lowest energies of  $K^-$  as functions of  $\rho_B$  for  $\Sigma_{Kn} = 305$  MeV (bold solid line) and  $\Sigma_{Kn} = 207$  MeV (thin solid line) in the case of H-EOS (A).

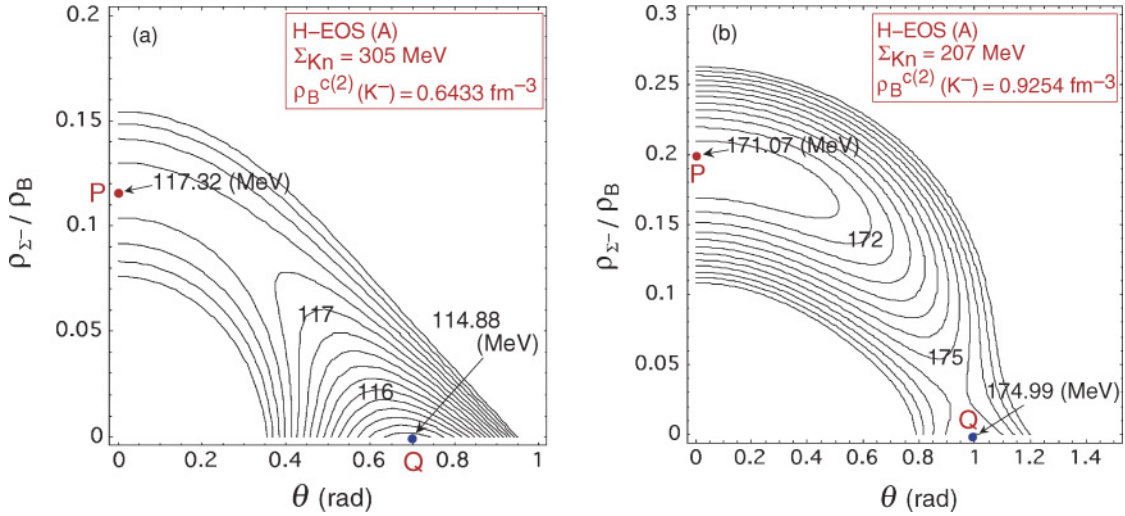


FIG. 4. (Color online) (a) Contour plot of the total energy per baryon  $\mathcal{E}'/\rho_B$  in the  $(\theta, \rho_{\Sigma^-}/\rho_B)$  plane at  $\rho_B = \rho_B^{c(2)}(K^-)$  for  $\Sigma_{Kn} = 305$  MeV in the case of H-EOS (A). The energy interval is taken to be 0.2 MeV. (b) The same as in (a), but for  $\Sigma_{Kn} = 207$  MeV. The energy interval is taken to be 0.5 MeV. See the text for details.

after the appearance of the negatively charged hyperon  $\Sigma^-$ , as seen in Fig. 3, so that the onset condition Eq. (1) is satisfied at a higher density than in the case of neutron-star matter without mixing of hyperons. We denote the density at which the lowest  $K^-$  energy  $\omega$  crosses the  $\mu$  as  $\rho_B^{c(2)}(K^-)$ . From Fig. 3, one reads  $\rho_B^{c(2)}(K^-) = 0.6433 \text{ fm}^{-3}$  ( $=4.02\rho_0$ ) for  $\Sigma_{Kn} = 305$  MeV and  $\rho_B^{c(2)}(K^-) = 0.9254 \text{ fm}^{-3}$  ( $=5.78\rho_0$ ) for  $\Sigma_{Kn} = 207$  MeV.

Now we examine whether the state at  $\rho_B = \rho_B^{c(2)}(K^-)$  is the true ground state by considering the dependence of the total energy of the system at  $\rho_B = \rho_B^{c(2)}(K^-)$  on the chiral angle  $\theta$  and  $\Sigma^-$ -mixing ratio  $\rho_{\Sigma^-}/\rho_B$ . In Fig. 4, the contour plots of the total energy per baryon  $\mathcal{E}'/\rho_B$  in the  $(\theta, \rho_{\Sigma^-}/\rho_B)$  plane at  $\rho_B = \rho_B^{c(2)}(K^-)$  are depicted for  $\Sigma_{Kn} = 305$  MeV [Fig. 4(a)] and  $\Sigma_{Kn} = 207$  MeV [Fig. 4(b)] in the case of H-EOS (A). Note that  $\mathcal{E}'/\rho_B$  has been maximized with respect to  $\mu$  and minimized with respect to the other remaining parameters  $\rho_\Lambda/\rho_B$  and  $\rho_p/\rho_B$ . The energy interval between the contours is taken to be 0.2 MeV for  $\Sigma_{Kn} = 305$  MeV and 0.5 MeV for  $\Sigma_{Kn} = 207$  MeV.

For  $\Sigma_{Kn} = 305$  MeV [Fig. 4(a)], one obtains a state satisfying the condition  $\omega = \mu$  at a point  $(\theta, \rho_{\Sigma^-}/\rho_B) = (0, 0.117)$ , where  $\mathcal{E}'/\rho_B = 117.32$  MeV (denoted as  $P$ ). However, this point is not a minimum but a saddle point in the  $(\theta, \rho_{\Sigma^-}/\rho_B)$  plane. A true minimum state exists at a different point,  $(\theta, \rho_{\Sigma^-}/\rho_B) = (0.70 \text{ rad}, 0)$ , in the plane (denoted as  $Q$ ). This state  $Q$  stands for the fully developed  $K^-$ -condensed state with no  $\Sigma^-$  mixing.

To see the mechanisms of how a true minimum state which has the fully developed  $K^-$  condensates with no  $\Sigma^-$  mixing appears, the total energy per baryon  $\mathcal{E}'/\rho_B$  of the kaon-condensed state and the contributions to  $\mathcal{E}'/\rho_B$  from each term on the right-hand side of Eq. (14) are shown in Fig. 5(a), as functions of the  $\Sigma^-$ -mixing ratio  $\rho_{\Sigma^-}/\rho_B$  at  $\rho_B = \rho_B^{c(2)}(K^-)$  ( $=0.6433 \text{ fm}^{-3}$ ) for  $\Sigma_{Kn} = 305$  MeV. At a given  $\rho_{\Sigma^-}/\rho_B$ , the total energy per baryon  $\mathcal{E}'/\rho_B$  is minimized with respect to  $\theta$ ,  $\rho_p$ , and  $\rho_\Lambda$ , and maximized with respect

to  $\mu$ . All the energy values are represented as the differences from the corresponding values at the state  $P$ . The state  $P$  satisfying the condition  $\omega = \mu$  corresponds to the point at  $\rho_{\Sigma^-}/\rho_B = 0.117$  on the bold solid line. The state  $Q$  denoting the absolute energy minimum with  $\theta = 0.70$  rad corresponds to the point at  $\rho_{\Sigma^-}/\rho_B = 0$  on the bold solid line. From comparison of each energy contribution at the states  $P$  and  $Q$ , one can see that the hyperon-nucleon ( $Y$ - $N$ ) mass difference mainly pushes up the total energy of the kaon-condensed state as the  $\Sigma^-$ -mixing ratio increases. The mixing of the  $\Sigma^-$  hyperon slightly reduces the total kinetic energy of baryons by lowering the Fermi momentum of each baryon, while slightly enlarging the baryon potential energy contribution. These two effects compensate each other. The lepton energy contribution is little changed by the  $\Sigma^-$  mixing. Note that the sum of the kaon-baryon scalar interaction energy and free kaon energy consisting of the kaon free mass and kinetic energy is positive, because the repulsive contribution from the free kaon energy surpasses the attractive interaction between kaons and baryons. As the  $\Sigma^-$ -mixing ratio increases, the fraction of the  $K^-$  condensates decreases, and so does the sum of the kaon-baryon scalar interaction energy and free kaon energy, because the negative charge of the  $K^-$  condensates is replaced by that of the  $\Sigma^-$  hyperons. However, the decrease in this repulsive effect from the  $K^-$  condensates to the energy cannot compensate for the energy excess from the  $Y$ - $N$  mass difference as the  $\Sigma^-$  mixing increases. As a result, the total energy of the kaon-condensed state increases monotonically with increase in the  $\Sigma^-$ -mixing ratio, and the state  $Q$  becomes the energy minimum, while the state  $P$  is the maximum with respect to the  $\Sigma^-$ -mixing ratio.

In the case of H-EOS (A) and  $\Sigma_{Kn} = 305$  MeV, the more detailed numerical analysis shows the following behavior for the energy minima in the  $(\theta, \rho_{\Sigma^-}/\rho_B)$  plane as the density  $\rho_B$  increases in the vicinity of  $\rho_B^{c(2)}(K^-)$ . At a certain density below  $\rho_B^{c(2)}(K^-)$ , a local minimum state  $Q'$  corresponding to the  $K^-$ -condensed state without the  $\Sigma^-$  mixing appears in

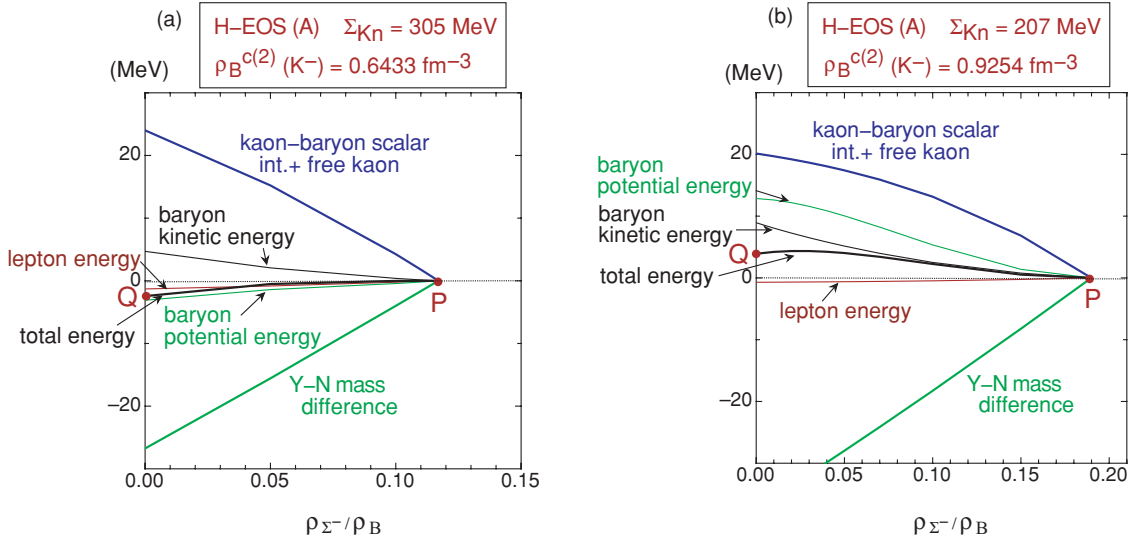


FIG. 5. (Color online) (a) Contributions from each term on the right-hand side of Eq. (14) to the total energy per baryon  $\mathcal{E}'/\rho_B$  as functions of the  $\Sigma^-$ -mixing ratio  $\rho_{\Sigma^-}/\rho_B$  at  $\rho_B = \rho_B^{c(2)}(K^-) (= 0.6433 \text{ fm}^{-3})$  for  $\Sigma_{Kn} = 305 \text{ MeV}$  (the solid lines). The H-EOS (A) is used for the hyperonic matter EOS. All the energy values are represented as the differences from the corresponding values at the state  $P$ . (b) The same as (a) but for  $\Sigma_{Kn} = 207 \text{ MeV}$  [ $\rho_B^{c(2)}(K^-) = 0.9254 \text{ fm}^{-3}$ ]. See the text for details.

addition to the absolute minimum state  $P'$  corresponding to the noncondensed state with the  $\Sigma^-$  mixing. [We denote this density as  $\rho_B^*(K^-; \text{no}\Sigma^-)$ .] As the density increases, the state  $Q'$  shifts to have a lower energy; and at a density denoted as  $\rho_B^{c(1)}(K^-; \text{no}\Sigma^-)$ , the energy values of the two minima  $P'$  and  $Q'$  become equal. Above  $\rho_B = \rho_B^{c(1)}(K^-; \text{no}\Sigma^-)$ , the state  $Q'$  becomes the absolute minimum, having a lower energy than that of the state  $P'$ . In Table II, we show the typical densities,  $\rho_B^*(K^-; \text{no}\Sigma^-)$  and  $\rho_B^{c(1)}(K^-; \text{no}\Sigma^-)$ , as well as  $\rho_B^{c(2)}(K^-)$ . In the case of H-EOS (A) and  $\Sigma_{Kn} = 305 \text{ MeV}$ , there is a *discontinuous* transition from the noncondensed state of hyperonic matter with the  $\Sigma^-$  mixing (the state  $P'$ ) to the  $K^-$ -condensed state without the  $\Sigma^-$  mixing (the state  $Q'$ ) above  $\rho_B = \rho_B^{c(1)}(K^-; \text{no}\Sigma^-)$ . This transition density  $\rho_B^{c(1)}(K^-; \text{no}\Sigma^-)$  is slightly lower than  $\rho_B^{c(2)}(K^-)$ .

Next we proceed to the case of H-EOS (A) and  $\Sigma_{Kn} = 207 \text{ MeV}$  (the weaker  $s$ -wave kaon-baryon scalar interaction). As seen from Fig. 4(b), the state  $P$  is an absolute minimum. Therefore, the assumption of the continuous transition is kept valid, and the onset density for kaon condensation is given by

$\rho_B^{c(2)}(K^-)$ . In Fig. 5(b), the total energy per baryon  $\mathcal{E}'/\rho_B$  of the kaon-condensed state and the contributions to  $\mathcal{E}'/\rho_B$  are shown as functions of the  $\Sigma^-$ -mixing ratio  $\rho_{\Sigma^-}/\rho_B$  for  $\Sigma_{Kn} = 207 \text{ MeV}$  [ $\rho_B^{c(2)}(K^-) = 0.9254 \text{ fm}^{-3}$ ]. The qualitative behaviors are the same as those for  $\Sigma_{Kn} = 305 \text{ MeV}$  [Fig. 5(a)] except for the baryon potential energy contribution, which decreases monotonically with increase in  $\rho_{\Sigma^-}/\rho_B$ . For this weaker  $s$ -wave kaon-baryon scalar interaction case, the critical density  $\rho_B^{c(2)}(K^-)$  is far beyond the onset density of  $\Sigma^-$ ,  $\rho_B^c(\Sigma^-) (= 0.52 \text{ fm}^{-3})$ . At such a high density, the baryon potential energy is lowered by the mixing of the  $\Sigma^-$ . Thus all the contributions except for the  $Y$ - $N$  mass difference term favor the  $\Sigma^-$  mixing, and the state  $P$  becomes the absolute minimum.

However, it should be noted that there still exists a kaon-condensed local minimum  $Q(\theta, \rho_{\Sigma^-}/\rho_B) = (1.0 \text{ rad}, 0)$  without the  $\Sigma^-$  mixing. Indeed, the local minimum (the state  $Q'$ ) exists from a fairly lower density  $\rho_B^*(K^-; \text{no}\Sigma^-) (= 0.8280 \text{ fm}^{-3})$  than  $\rho_B^{c(2)}(K^-) (= 0.9254 \text{ fm}^{-3})$  (see Table II).

TABLE II. Typical densities associated with the appearance of  $K^-$  condensates and  $\Sigma^-$  hyperons. They are calculated with the EOS models for hyperonic matter, H-EOS (A) and H-EOS (B). The values in parentheses for  $\rho_B^{c(2)}(K^-)$  do not correspond to the true energy minimum but to the local minimum or the saddle point in the  $(\theta, \rho_{\Sigma^-}/\rho_B)$  plane. See the text for details.

H-EOS	$\Sigma_{Kn}$ (MeV)	$\rho_B^*(K^-; \text{no}\Sigma^-)$ ( $\text{fm}^{-3}$ )	$\rho_B^{c(1)}(K^-; \text{no}\Sigma^-)$ ( $\text{fm}^{-3}$ )	$\rho_B^{c(2)}(K^-)$ ( $\text{fm}^{-3}$ )	$\rho_B^*(K^-; \Sigma^-)$ ( $\text{fm}^{-3}$ )	$\rho_B^{c(1)}(K^-; \Sigma^-)$ ( $\text{fm}^{-3}$ )
(A)	305	0.5782	0.6135	(0.6433)	1.011	1.039
	207	0.8280	—	0.9254	—	—
(B)	305	—	—	0.5504	1.006	1.069
	207	0.7084	0.9086	(0.9189)	0.9189	1.170



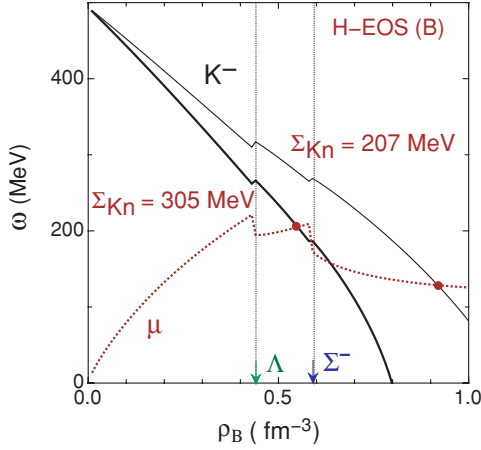


FIG. 6. (Color online) Lowest energies of  $K^-$  as functions of  $\rho_B$  for  $\Sigma_{Kn} = 305$  MeV (bold solid line) and  $\Sigma_{Kn} = 207$  MeV (thin solid line) in the case of H-EOS (B).

### B. Case of H-EOS (B)

In the case of H-EOS (B) for the hyperonic matter EOS, both the  $\Lambda$  and  $\Sigma^-$  start to be mixed at higher densities than in the case of H-EOS (A) (Sec. III). In Fig. 6, we show the lowest energies of the  $K^-$  as functions of baryon number density  $\rho_B$  for  $\Sigma_{Kn} = 305$  and 207 MeV.

In Fig. 7, the contour plots of the total energy per baryon  $\mathcal{E}'/\rho_B$  in the  $(\theta, \rho_{\Sigma^-}/\rho_B)$  plane at  $\rho_B = \rho_B^{c(2)}(K^-)$  are depicted for  $\Sigma_{Kn} = 305$  and 207 MeV in the case of H-EOS (B).

From Fig. 6, the critical density  $\rho_B^{c(2)}(K^-)$  is read as  $0.5504 \text{ fm}^{-3} (=3.44\rho_0)$  for  $\Sigma_{Kn} = 305$  MeV and as  $0.9189 \text{ fm}^{-3} (=5.74\rho_0)$  for  $\Sigma_{Kn} = 207$  MeV.

For  $\Sigma_{Kn} = 305$  MeV, the condition  $\omega = \mu$  [Eq. (1)] is satisfied before  $\Sigma^-$  mixing starts, i.e.,  $\rho_B^{c(2)}(K^-) < \rho_B^c(\Sigma^-)$ . As seen from Fig. 7(a), the corresponding state  $P$  is the absolute minimum for the total energy per baryon  $\mathcal{E}'/\rho_B$  in

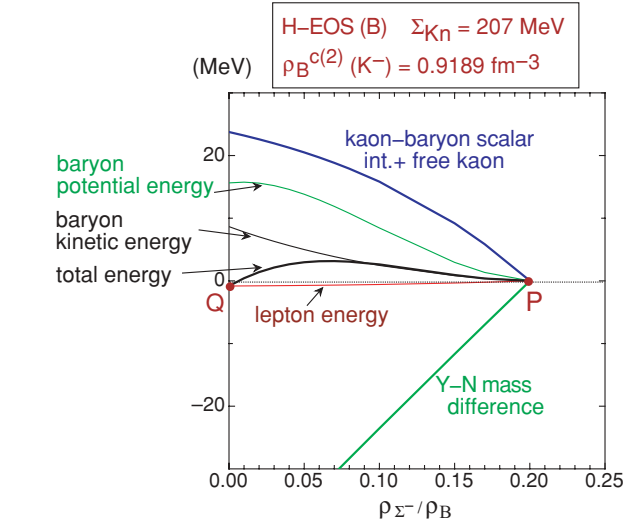
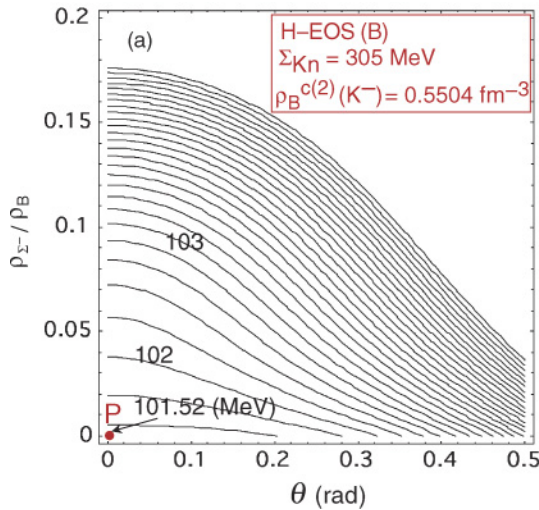


FIG. 8. (Color online) Same as Fig. 5(b) but for H-EOS (B) and  $\Sigma_{Kn} = 207$  MeV [ $\rho_B^{c(2)}(K^-) = 0.9189 \text{ fm}^{-3}$ ]. See the text for details.

the  $(\theta, \rho_{\Sigma^-}/\rho_B)$  plane at  $\rho_B = \rho_B^{c(2)}(K^-)$ , and there is no local minimum with kaon condensates without the  $\Sigma^-$  mixing. Therefore, the assumption of the continuous phase transition does not lose its validity when the  $\Sigma^-$  hyperons are not mixed in the ground state.

On the other hand, for  $\Sigma_{Kn} = 207$  MeV, the state  $P$  satisfying the condition  $\omega = \mu$  is obtained as a local minimum at a point  $(\theta, \rho_{\Sigma^-}/\rho_B) = (0, 0.200)$  in the presence of the  $\Sigma^-$ , and there is an absolute minimum with kaon condensates without the  $\Sigma^-$  mixing (the state  $Q$  in Fig. 7(b)) at a point  $(\theta, \rho_{\Sigma^-}/\rho_B) = (1.02 \text{ rad}, 0)$ . The total energy per baryon  $\mathcal{E}'/\rho_B$  of the kaon-condensed state and the contributions to  $\mathcal{E}'/\rho_B$  from each term on the right-hand side of Eq. (14) are also shown in Fig. 8, as functions of the  $\Sigma^-$ -mixing ratio  $\rho_{\Sigma^-}/\rho_B$  at  $\rho_B = \rho_B^{c(2)}(K^-) (=0.9189 \text{ fm}^{-3})$  for H-EOS (B) and  $\Sigma_{Kn} = 207$  MeV.

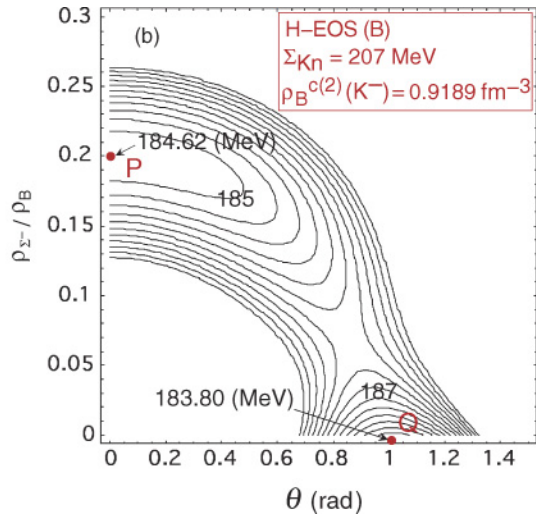


FIG. 7. (Color online) (a) Contour plot of the total energy per baryon  $\mathcal{E}'/\rho_B$  in the  $(\theta, \rho_{\Sigma^-}/\rho_B)$  plane at  $\rho_B = \rho_B^{c(2)}(K^-)$  for  $\Sigma_{Kn} = 305$  MeV in the case of H-EOS (B). The energy interval is taken to be 0.2 MeV. (b) The same as in (a), but for  $\Sigma_{Kn} = 207$  MeV. The energy interval is taken to be 0.5 MeV. See the text for details.

The qualitative behavior for each contribution is similar to that in Fig. 5(b) for H-EOS (A) and  $\Sigma_{Kn} = 207$  MeV. However, competition between the  $\Sigma^-$  and  $K^-$  condensates is more remarkable than in the case of H-EOS (A) and  $\Sigma_{Kn} = 207$  MeV, making the state  $Q$  energetically more favorable than the state  $P$ . From Table II, one can see the common behavior as in the case of H-EOS (A) and  $\Sigma_{Kn} = 305$  MeV concerning the appearance of  $K^-$  condensates and  $\Sigma^-$  hyperons, that is, there is a *discontinuous* transition from the noncondensed state of hyperonic matter with the  $\Sigma^-$  mixing to the  $K^-$ -condensed state without the  $\Sigma^-$  mixing above  $\rho_B = \rho_B^{c(1)}(K^-; \text{no } \Sigma^-)$ , and this transition density  $\rho_B^{c(1)}(K^-; \text{no } \Sigma^-)$  is slightly lower than  $\rho_B^{c(2)}(K^-)$ .

## V. EQUATION OF STATE

### A. Two energy minima with and without $\Sigma^-$ mixing for the $K^-$ -condensed phase

Here we discuss the EOS of the  $K^-$ -condensed phase in hyperonic matter. The total energies per baryon in the  $K^-$ -condensed phase,  $\mathcal{E}'/\rho_B$ , as functions of the baryon number density  $\rho_B$  are shown in Fig. 9 for H-EOS (A) and H-EOS (B). In each case of the model EOS for hyperonic matter and the  $Kn$  sigma term  $\Sigma_{Kn}$ , there are two solutions of the kaon-condensed phase corresponding to two minima in the  $(\theta, \rho_{\Sigma^-}/\rho_B)$  plane at some density intervals. One is the  $K^-$ -condensed state without  $\Sigma^-$  mixing (dashed lines) called the state  $Q'$  in Sec. IV, and the other is with  $\Sigma^-$  mixing (solid lines), which we call the state  $R'$ . The density at which the state  $R'$  appears as a local minimum is denoted as  $\rho_B^*(K^-; \Sigma^-)$ . For example, we show in Fig. 10 the contour plots of  $\mathcal{E}'/\rho_B$  in the  $(\theta, \rho_{\Sigma^-}/\rho_B)$  plane at  $\rho_B = \rho_B^*(K^-; \Sigma^-)$  for  $\Sigma_{Kn} = 305$  MeV for H-EOS (A) and H-EOS (B).

In Fig. 11, we show the dependence of the baryon potentials  $V_{\Sigma^-}$ ,  $V_n$ , the neutron chemical potential  $\mu_n$ , and the difference

of the  $\Sigma^-$  and charge chemical potentials,  $\mu_{\Sigma^-} - \mu$ , on the  $\Sigma^-$ -mixing ratio  $\rho_{\Sigma^-}/\rho_B$  in the kaon-condensed phase at  $\rho_B = \rho_B^*(K^-; \Sigma^-)$  for  $\Sigma_{Kn} = 305$  MeV with H-EOS (A) and with H-EOS (B).

One can see that the chemical potential difference  $\mu_{\Sigma^-} - \mu$  has a minimum at a finite value of  $\rho_{\Sigma^-}/\rho_B (=0.12-0.14)$  and that the neutron chemical potential  $\mu_n$  decreases monotonically with increase in the  $\Sigma^-$ -mixing ratio within the range  $\rho_{\Sigma^-}/\rho_B = 0.0-0.3$ . As a result, the chemical equilibrium condition,  $\mu_n = \mu_{\Sigma^-} - \mu$ , for the weak process  $ne^- \rightleftharpoons \Sigma^-(\nu_e)$  is met at a finite  $\Sigma^-$ -mixing ratio ( $=0.07-0.1$ ), where the state  $R'$  in Fig. 10 appears. The dependence of the chemical potentials  $\mu_{\Sigma^-} - \mu$  and  $\mu_n$  on the  $\Sigma^-$ -mixing ratio is caused by that of the baryon potentials  $V_{\Sigma^-}$  and  $V_n$ , respectively, as seen from Fig. 11.

Except for the case of  $\Sigma_{Kn} = 207$  MeV with H-EOS (A) where the  $\Sigma^-$  hyperons are already mixed at the onset density of the  $K^-$  condensates, the difference of the energies between the state  $R'$  and the absolute minimum state  $Q'$  gets smaller as the density increases. And at a certain density denoted as  $\rho_B^{c(1)}(K^-; \Sigma^-)$ , the energies of the states  $Q'$  and  $R'$  become equal. Above the density  $\rho_B^{c(1)}(K^-; \Sigma^-)$ , the state  $R'$  develops as an absolute energy minimum. In Table II, we show the numerical values of  $\rho_B^*(K^-; \Sigma^-)$  and  $\rho_B^{c(1)}(K^-; \Sigma^-)$  for each case of  $\Sigma_{Kn}$  and the hyperonic matter EOS.

At a given density, the ground state is determined by the lowest energy state in Fig. 9. For all the cases, the state  $R'$  becomes the ground state at higher densities, i.e., the  $\Sigma^-$  is mixed in the fully developed kaon-condensed phase. Except for the case of  $\Sigma_{Kn} = 207$  MeV with H-EOS (A), the transition from the  $Q'$  state (the dashed lines) to the  $R'$  state (the solid lines) is discontinuous. Even when the state  $R'$  is the ground state, the local minimum (the state  $Q'$ ) prevails over the wide range of the baryon number density, in particular, in the case of H-EOS (B) [see the dashed lines in Fig. 9(b)].

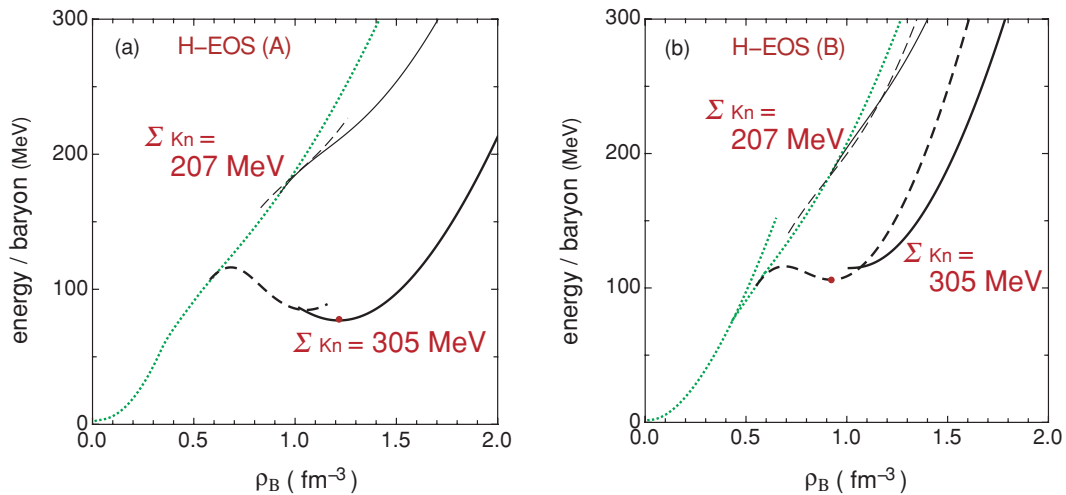


FIG. 9. (Color online) Total energies per baryon  $\mathcal{E}'/\rho_B$  in the  $K^-$ -condensed phase as functions of  $\rho_B$  for (a) H-EOS (A) and (b) H-EOS (B). The bold (thin) lines are for  $\Sigma_{Kn} = 305$  MeV ( $\Sigma_{Kn} = 207$  MeV). The solid lines stand for the total energies per baryon for the  $K^-$ -condensed state with  $\Sigma^-$  mixing, while the dashed lines for the  $K^-$ -condensed state without  $\Sigma^-$  mixing. For comparison,  $\mathcal{E}'/\rho_B$  for the noncondensed hyperonic matter is shown by the dotted lines.

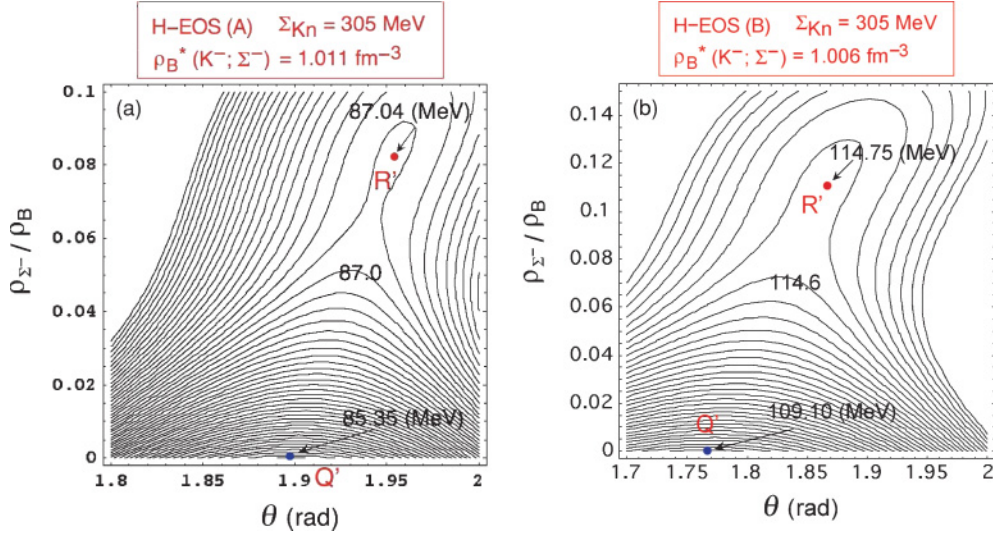


FIG. 10. (Color online) Contour plots of the total energy per baryon  $\mathcal{E}'/\rho_B$  in the  $(\theta, \rho_{\Sigma^-}/\rho_B)$  plane at  $\rho_B = \rho_B^*(K^-; \Sigma^-)$  for  $\Sigma_{Kn} = 305$  MeV in the case of (a) H-EOS (A) with an energy interval of 0.05 MeV, and (b) H-EOS (B) with an energy interval of 0.2 MeV. See the text for details.

In Fig. 12, we show the pressure in the  $K^-$ -condensed phase obtained by  $P \equiv \rho_B^2 \partial(\mathcal{E}'/\rho_B)/\partial\rho_B (= -\mathcal{E}'_{\text{eff}})$ , as functions of the energy density,  $\epsilon \equiv \mathcal{E}' + M_N \rho_B$ , in  $\text{MeV fm}^{-3}$ , for both H-EOS (A) and (B). The bold (thin) lines are for  $\Sigma_{Kn} = 305$  MeV ( $\Sigma_{Kn} = 207$  MeV). The solid lines stand for the pressure for the  $K^-$ -condensed state with the  $\Sigma^-$  mixing, while the dashed lines for the  $K^-$ -condensed state without the  $\Sigma^-$  mixing. For comparison, the pressure for the non-condensed hyperonic matter is shown by the dotted line. Except for the case of  $\Sigma_{Kn} = 207$  MeV with H-EOS (A), there appears a gap in the pressure at the transition density  $\rho_B^{c(1)}(K^-; \Sigma^-)$  as a result of the discontinuous transition. Note that the speed of sound  $(\partial P/\partial\epsilon)^{1/2}$  exceeds the speed of light  $c$  above a certain energy density, which is denoted as an arrow for each corresponding pressure curve. In such high-density regions, the relativistically covariant formulation is necessary for quantitative discussion of the EOS.

#### B. Density isomer state in the case of the stronger $s$ -wave kaon-baryon scalar attraction

In the kaon-condensed phase realized in hyperonic matter, the EOS becomes considerably soft. In particular, in the case of  $\Sigma_{Kn} = 305$  MeV for both H-EOS (A) and (B), a local energy minimum (which we call the density isomer state) appears at a certain density  $\rho_{B,\text{min}}$  denoted as dots in Figs. 9 and 12, and the pressure becomes negative at some density intervals below  $\rho_{B,\text{min}}$ . For H-EOS (A) [H-EOS (B)], one reads  $\rho_{B,\text{min}} = 1.22 \text{ fm}^{-3}$  ( $0.92 \text{ fm}^{-3}$ ), and the minimum energy per baryon at  $\rho_{B,\text{min}}$  is 76.9 MeV (106.1 MeV) (see Fig. 9). The energy at  $\rho_{B,\text{min}}$  is smaller than the  $\Lambda$ - $N$  mass difference,  $\delta M_{\Lambda N} = 176$  MeV. Thus the density isomer state is stable against the strong decay processes.

To clarify mechanisms for the significant softening of the EOS leading to the appearance of the local energy minimum and for subsequent recovering of the stiffness of the EOS

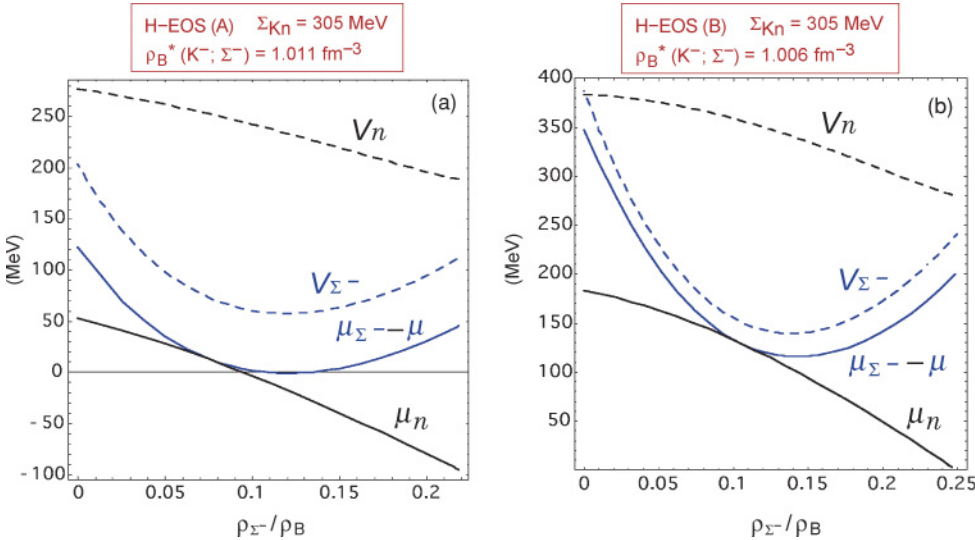


FIG. 11. (Color online) Dependence of  $V_{\Sigma^-}$ ,  $V_n$ , and  $\mu_{\Sigma^-} - \mu$ ,  $\mu_n$  on the  $\Sigma^-$ -mixing ratio  $\rho_{\Sigma^-}/\rho_B$  in the kaon-condensed phase at  $\rho_B = \rho_B^*(K^-; \Sigma^-)$  for  $\Sigma_{Kn} = 305$  MeV with (a) H-EOS (A) and (b) H-EOS (B).

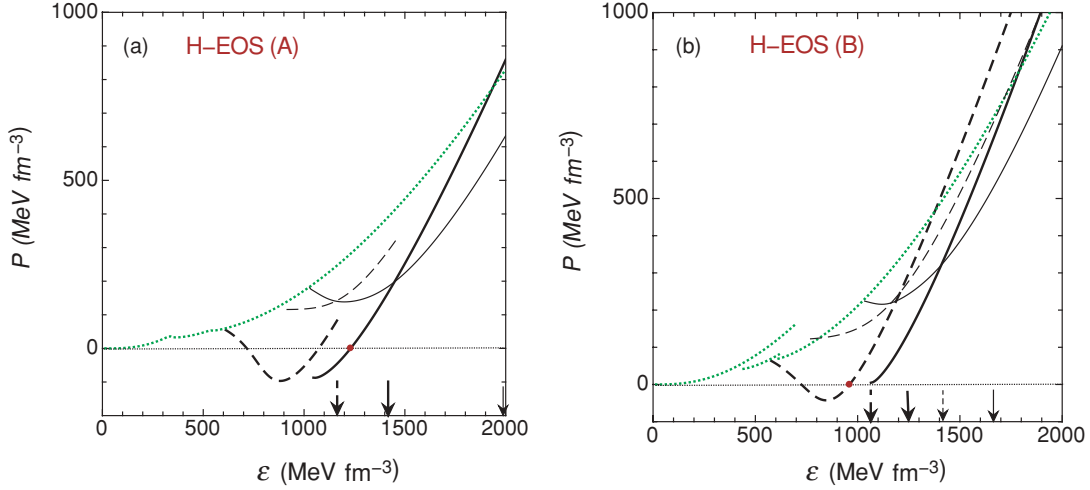


FIG. 12. (Color online) Pressure ( $\text{MeV fm}^{-3}$ ) in the  $K^-$ -condensed phase,  $P \equiv \rho_B^2 \partial(\mathcal{E}'/\rho_B)/\partial \rho_B (= -\mathcal{E}'_{\text{eff}})$ , as function of energy density  $\epsilon$  ( $\text{MeV fm}^{-3}$ ) for (a) H-EOS (A) and (b) H-EOS (B). Line notation is the same as in Fig. 9.

at higher density regions, we show the energy contributions to the total energy per baryon by the solid lines in the case of  $\Sigma_{Kn} = 305$  MeV for H-EOS (A) and (B) in Fig. 13. For comparison, those for the kaon-condensed phase realized in ordinary neutron-star matter, obtained after putting  $\rho_\Lambda = \rho_{\Sigma^-} = 0$ , are shown by the dashed lines. The density region where the total energy per baryon decreases with density (i.e., the negative pressure region) is bounded by the vertical dotted lines in Figs. 13(a) and 13(b).

The dependence of the total energy on the baryon number density is mainly determined by the two contributions: (I) the contribution from the classical kaons as the sum of the  $s$ -wave scalar kaon-baryon interaction and the free parts of the condensed kaon energy [the fourth, fifth, and sixth terms in Eq. (14)] and (II) the baryon potential energy  $\mathcal{E}_{\text{pot}}/\rho_B$  [the

third term in Eq. (14)]. Both the attractive energy contribution (I) and the repulsive energy contribution (II) become large with increased density. As one can see by comparing the solid and dashed lines in Fig. 13, the attractive effect from contribution (I) is more pronounced because of hyperon mixing than in the case without hyperons, thus lowering the total energy at a given density. In addition, the repulsive effect from the contribution (II) is much weakened by hyperon mixing at a given density, since the repulsive interaction between nucleons is avoided by lowering the relative nucleon density through hyperon mixing.<sup>7</sup> As a result of these two effects, mixing of

<sup>7</sup>This suppression mechanism of the repulsive interaction between nucleons is essentially the same as that for softening of the EOS in the noncondensed hyperonic matter as pointed out in Refs. [37,38].

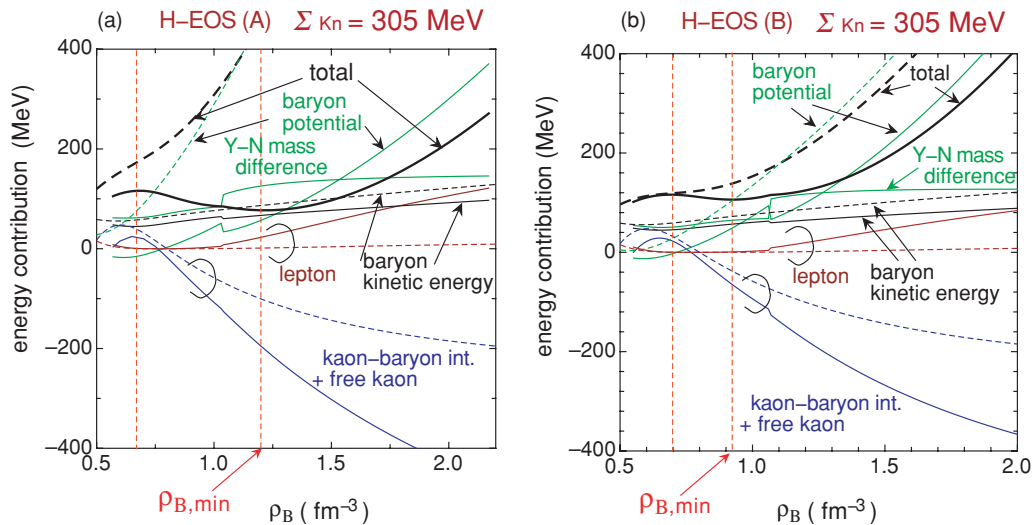


FIG. 13. (Color online) Contributions to the total energy per baryon for the kaon-condensed phase in hyperonic matter as functions of the baryon number density  $\rho_B$  for  $\Sigma_{Kn} = 305$  MeV (solid lines) with (a) H-EOS (A) and (b) H-EOS (B). For comparison, those for the kaon-condensed phase realized in ordinary neutron-star matter, obtained after putting  $\rho_\Lambda = \rho_{\Sigma^-} = 0$ , are shown by the dashed lines. See the text for details.



hyperons leads to significant softening of the EOS for the kaon-condensed phase in hyperonic matter.

In the kaon-condensed phase in hyperonic matter (solid lines in Fig. 13), the increase of the absolute value of the kaon-baryon attractive interaction with density is more remarkable than the increase of the potential energy with density at the density intervals bounded by the vertical dotted lines in Fig. 13. The density dependence of the other energy contributions is small. As a result, the total energy per baryon decreases with density in this density region, and there is an energy minimum at  $\rho_{B,\min}$ . At higher densities above  $\rho_{B,\min}$ , the decrease of the contribution (I) gets slightly moderate, while the increase of the contribution (II) with density becomes more marked because of the increase of the repulsion between baryons. Therefore, the total energy per baryon increases rapidly with density, and the EOS recovers the stiffness at very high densities. The stiffness of the EOS depends on the quantitative behavior of the repulsive interaction between baryons at high densities, which has ambiguity depending on the model interaction. In our framework, the H-EOS (B) brings about a stiffer EOS at high densities than the H-EOS (A), since the many-body hyperon-nucleon and hyperon-hyperon repulsive interaction terms, which control the stiffness of the EOS at high densities, contribute more significantly in the H-EOS (B) (the exponent  $\gamma = 2.0$ ) than in the H-EOS(A) ( $\gamma = 5/3$ ).

It has been suggested in Ref. [59] that a density isomer state with kaon condensates in hyperonic matter implies the existence of self-bound objects, which can be bound essentially without gravitation on a scale of an atomic nucleus to a neutron star just like a strangelet and a strange star [60–64] or other exotic matter [65–69]. The density isomer state is located at a local energy minimum with respect to the baryon number density as a metastable state, but it decays only through multiple weak processes, so it is regarded as substantially stable. Implications of such self-bound objects with kaon condensates for astrophysical phenomena and nuclear experiments will be discussed in detail in a subsequent paper, where both

$s$ -wave and  $p$ -wave kaon-baryon interactions are taken into account [46].

### C. Composition of matter in the kaon-condensed phase

The characteristic features of the kaon-condensed phase in hyperonic matter can be surveyed from the density dependence of the composition of matter. In Figs. 14 and 15, the particle fractions  $\rho_i/\rho_B$  ( $i = p, \Lambda, n, \Sigma^-, K^-, e^-$ ) are shown as functions of the baryon number density  $\rho_B$ , with  $\Sigma_{Kn} = 305$  MeV and  $\Sigma_{Kn} = 207$  MeV, for H-EOS(A) (Fig. 14) and H-EOS(B) (Fig. 15). The long dashed lines stand for the ratio of the total negative strangeness number density  $\rho_{\text{strange}}$  to the baryon number density  $\rho_B$  with

$$\rho_{\text{strange}} = \rho_{K^-} + \rho_{\Lambda} + \rho_{\Sigma^-}, \quad (24)$$

where  $\rho_{K^-}$  is given by Eq. (18). The contribution from the classical kaon part,  $\rho_{K^-}/\rho_B$ , is shown by the short dashed line in each figure.

For each curve in Figs. 14 and 15, only the quantity corresponding to the lowest energy minimum state in the  $(\theta, \rho_{\Sigma^-}/\rho_B)$  plane is shown as a function of density, so there are gaps in the quantities at the transition densities  $\rho_B^{c(1)}(K^-; \text{no } \Sigma^-)$  and  $\rho_B^{c(1)}(K^-; \Sigma^-)$ . One can see competing effects between kaon condensates and  $\Sigma^-$  hyperons: as the former develops around the density  $\rho_B^{c(1)}(K^-; \text{no } \Sigma^-)$ , the latter is suppressed, while as the latter develops in the kaon-condensed phase around the density  $\rho_B^{c(1)}(K^-; \Sigma^-)$ , the former is suppressed.

Appearance of both kaon condensates and the  $\Sigma^-$  leads to considerable suppression of the electron fraction, since the negative charge of the electron is replaced by that of kaon condensates and  $\Sigma^-$  hyperons. Accordingly, the charge chemical potential  $\mu$  decreases with an increase in the baryon number density through the relation  $\rho_e = \mu^3/(3\pi^2)$ . It becomes even negative above the density  $\rho_B = 0.77 \text{ fm}^{-3}$  for

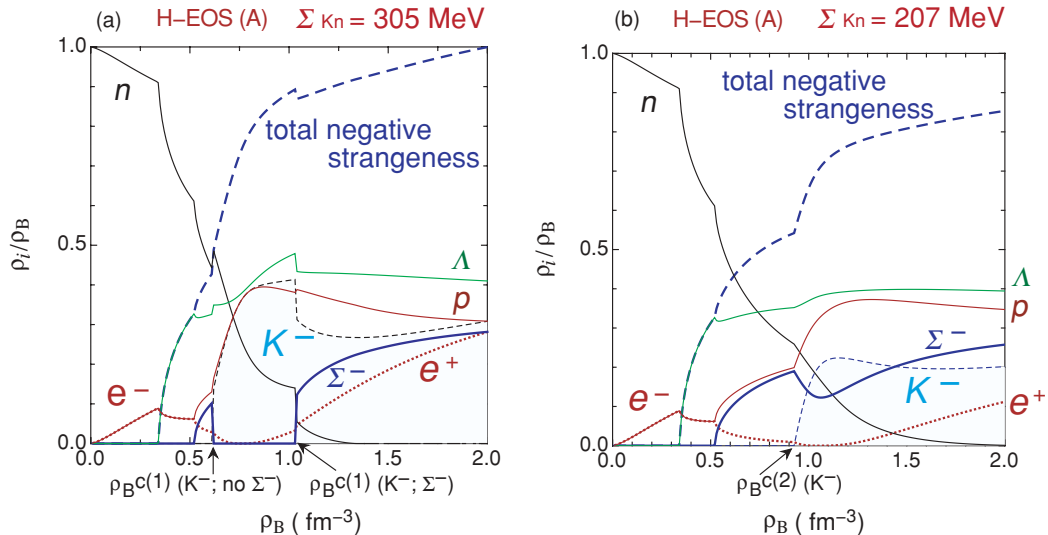


FIG. 14. (Color online) Particle fractions  $\rho_i/\rho_B$  in the  $K^-$ -condensed phase as functions of  $\rho_B$  for H-EOS (A) and (a)  $\Sigma_{Kn} = 305$  and (b)  $\Sigma_{Kn} = 207$  MeV.

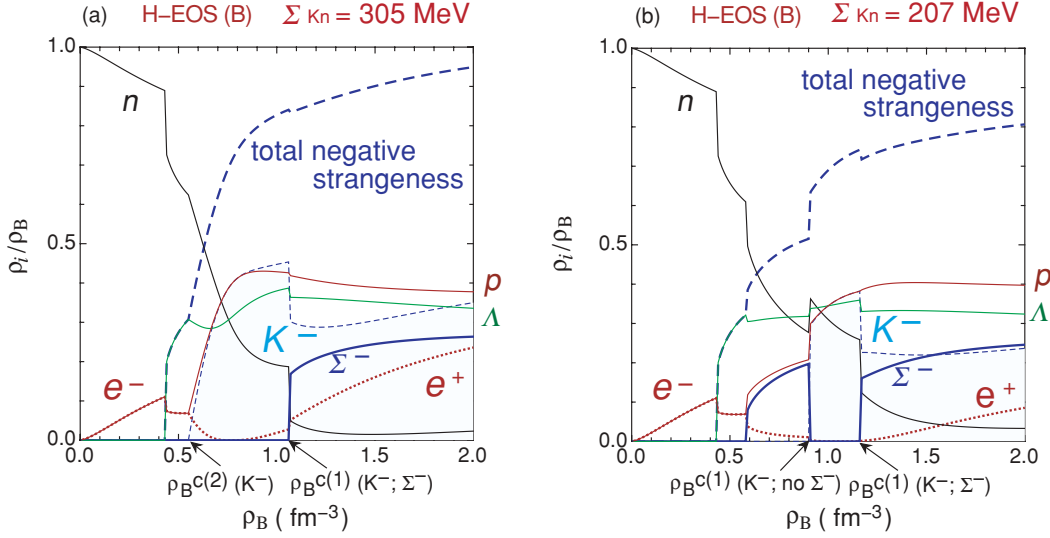


FIG. 15. (Color online) Same as Fig. 14, but for H-EOS (B).

$\Sigma_{Kn} = 305$  MeV and  $\rho_B = 1.06 \text{ fm}^{-3}$  for  $\Sigma_{Kn} = 207$  MeV for both H-EOS (A) and (B). For  $\mu < 0$ , the positrons ( $e^+$ ) appear in place of the electrons.

At high densities, the protons,  $\Lambda$ , and  $\Sigma^-$  hyperons are equally populated in the kaon-condensed phase, i.e.,  $\rho_p/\rho_B, \rho_\Lambda/\rho_B, \rho_{\Sigma^-}/\rho_B = 30\text{--}40\%$ , whereas the neutrons almost disappear. The total negative strangeness ratio,  $\rho_{\text{strange}}/\rho_B$ , becomes larger with an increase in density. It reaches almost unity for  $\Sigma_{Kn} = 305$  MeV and 0.8–0.9 for  $\Sigma_{Kn} = 207$  MeV at high densities for both H-EOS (A) and (B). Such a high strangeness fraction implies a close connection between the kaon-condensed phase in hyperonic matter and strange matter where  $u, d$ , and  $s$  quarks are almost equally populated in quark matter.

## VI. SUMMARY AND CONCLUDING REMARKS

We have studied the  $s$ -wave kaon condensation realized in hyperonic matter based on chiral symmetry for the kaon-baryon interactions and taking into account the parametrized effective interactions between baryons. We have concentrated on the interrelations between kaon condensates and negatively charged hyperons ( $\Sigma^-$ ) and reexamined the validity of the assumption of the continuous phase transition from the noncondensed hyperonic matter to the  $K^-$ -condensed phase. We have also discussed the EOS and the characteristic features of the system for the fully developed kaon-condensed phase.

The validity of the continuous phase transition for kaon condensation in hyperonic matter is summarized as follows. In cases where the condition  $\omega = \mu$  [Eq. (1)] is satisfied at  $\rho_B = \rho_B^{c(2)}(K^-)$  in the presence of the  $\Sigma^-$  hyperons, there exist, in general, two energy minima in the  $(\theta, \rho_{\Sigma^-}/\rho_B)$  plane at some density intervals near the density  $\rho_B^{c(2)}(K^-)$ . One is the noncondensed state with the  $\Sigma^-$  mixing ( $P'$ ), and the other is the  $K^-$ -condensed state without the  $\Sigma^-$  mixing ( $Q'$ ). If the density  $\rho_B^{c(2)}(K^-)$  is located near the onset density of the  $\Sigma^-$ ,  $\rho_B^c(\Sigma^-)$ , the state  $P'$  is a local minimum or a saddle point,

and the state  $Q'$  is the absolute minimum at  $\rho_B = \rho_B^{c(2)}(K^-)$ . In this case, the assumption of the continuous phase transition is not valid. Below  $\rho_B^{c(2)}(K^-)$ , there exists a typical density  $\rho_B^{c(1)}(K^-; \text{no } \Sigma^-)$  at which the energies of the two minima become equal. Above the density  $\rho_B^{c(1)}(K^-; \text{no } \Sigma^-)$ , there is a discontinuous transition from the state  $P'$  to the state  $Q'$ . On the other hand, if the density  $\rho_B^{c(2)}(K^-)$  is located high enough above the density  $\rho_B^c(\Sigma^-)$ , the state  $P'$  is always an absolute minimum. In this case, the assumption of the continuous phase transition holds true, and the onset density of kaon condensation is given by  $\rho_B^{c(2)}(K^-)$ , above which kaon condensates develop continuously with increase in the baryon number density.

When the condition  $\omega = \mu$  is satisfied in the absence of the  $\Sigma^-$  hyperon, there exists a unique minimum of the noncondensed state ( $P'$ ) at a point (0,0) in the  $(\theta, \rho_{\Sigma^-}/\rho_B)$  plane, and the assumption of the continuous phase transition is kept valid. The onset density is given by  $\rho_B^{c(2)}(K^-)$ .

The above consequences on the validity of the continuous phase transition are expected to be general and should also be applied to cases where the other negatively charged hyperons such as the cascade  $\Xi^-$  are present in the noncondensed ground state and where both the  $s$ -wave and  $p$ -wave kaon-baryon interactions are taken into account [46].

In the fully developed phase with kaon condensates, there exist two energy minima with and without the  $\Sigma^-$  mixing in the  $(\theta, \rho_{\Sigma^-}/\rho_B)$  plane at some density intervals. At higher densities, the ground state is transferred discontinuously from the kaon-condensed state without the  $\Sigma^-$  mixing to that with the  $\Sigma^-$  mixing, except for the case of H-EOS (A) with the weaker  $s$ -wave kaon-baryon attractive interaction. The EOS of the kaon-condensed phase becomes considerably soft, since both the kaon-baryon attractions and mixing of hyperons work to lower the energy of the system. At higher densities, the stiffness of the EOS is recovered because of the increase in the repulsive interaction between baryons. As a result, in the case of the stronger  $s$ -wave kaon-baryon attractive interaction ( $\Sigma_{Kn} =$

305 MeV), there appears a local energy minimum as a density isomer state, which suggests the existence of self-bound objects with kaon condensates on any scale from an atomic nucleus to a neutron star. Recently, deeply bound kaonic nuclear states have been proposed theoretically, and much discussion has been made about the experimental achievements with them [70–80]. In particular, the double and/or multiple kaon clusters advocated in the recent experimental proposal by way of invariant mass spectroscopy [72] may have a close connection with our results of kaon-condensed self-bound objects. These experimental searches for deeply bound kaonic nuclear states may provide us with important information on the existence of kaon condensation in high-density matter.

In this paper, both kinematics and interactions associated with baryons are treated nonrelativistically. For more quantitative consideration, one needs a relativistic framework. Specifically, the  $s$ -wave kaon-baryon scalar attraction, which is proportional to the scalar densities for baryons in the relativistic framework, is suppressed at high densities because of the saturation of the scalar densities [5]. This effect is expected to make the EOS stiffer at high densities.

The kaon-condensed phase is important in understanding the high-density QCD phase diagram from a hadronic picture which we have taken over the relevant baryon densities. At high densities, however, quark degrees of freedom may appear explicitly. It has been shown in this paper that the kaon-condensed phase in hyperonic matter leads to a large (negative) strangeness fraction,  $\rho_{\text{strange}}/\rho_B \sim 1$ . This result suggests that the kaon-condensed phase in the hadronic picture may be considered as a pathway to strange quark matter. In a quark picture, a variety of deconfined quark phases including color superconductivity have been elaborated [81]. In particular, kaonic modes may be condensed in the color-flavor locked phase [82–85]. It would be interesting to clarify the relationship between kaon condensation in the hadronic phase and that in the quark phase and the possible transition between the two phases [86].

## ACKNOWLEDGMENTS

The author is grateful to T. Tatsumi, T. Takatsuka, T. Kunihiro, and M. Sugawara for valuable discussions. He also thanks the Yukawa Institute for Theoretical Physics at Kyoto University, where this work was completed during the YKIS 2006 on “New Frontiers on QCD.” This work is supported in part by the Grant-in-Aid for Scientific Research Fund (C) of the Ministry of Education, Science, Sports, and Culture (No. 18540288), and by the funds provided by Chiba Institute of Technology.

## APPENDIX: ONSET CONDITIONS OF $\Lambda$ AND $\Sigma^-$ HYPERONS IN ORDINARY NEUTRON-STAR MATTER

We recapitulate how hyperons  $\Lambda$  and  $\Sigma^-$  appear in the ordinary neutron-star matter composed of protons, neutrons,

and leptons within the baryon-baryon interaction models H-EOS (A) and (B). In particular, we compare onset mechanisms of the hyperon mixing between H-EOS (A) and (B).

### A. $\Lambda$ -mixing

The condition of the  $\Lambda$  mixing in the noncondensed neutron-star matter is given by Eq. (20b) with  $\theta = 0$ , that is,  $\mu_\Lambda = \mu_n$  with

$$\mu_\Lambda = \frac{(3\pi^2 \rho_\Lambda)^{2/3}}{2M_N} + \delta M_{\Lambda N} + V_\Lambda, \quad (\text{A1a})$$

$$\mu_n = \frac{(3\pi^2 \rho_n)^{2/3}}{2M_N} + V_n, \quad (\text{A1b})$$

together with  $\mu_n = \mu_p + \mu$  [Eq. (20a) with  $\theta = 0$ ] and the charge neutrality condition,  $\rho_p = \rho_e$ .

In Fig. 16, the baryon potentials  $V_\Lambda$  and  $V_n$ , the chemical potentials  $\mu_\Lambda$  and  $\mu_n$ , and the total energy per baryon  $\mathcal{E}'/\rho_B$  are shown as functions of the  $\Lambda$  mixing ratio  $\rho_\Lambda/\rho_B$  at the minimal baryon number density  $\rho_B^*(\Lambda)$  above which the  $\Lambda$ -mixing condition,  $\mu_\Lambda = \mu_n$ , is satisfied, for both H-EOS (A) and (B). For H-EOS (A), the condition  $\mu_\Lambda = \mu_n$  is met at  $\rho_\Lambda/\rho_B = 0$ , where  $\mathcal{E}'/\rho_B$  is a minimum. Therefore, the  $\Lambda$  hyperon starts to be mixed continuously in the ground state of  $(n, p, e^-)$  matter at this density  $\rho_B^*(\Lambda)(=0.340 \text{ fm}^{-3})$ , which gives the onset density  $\rho_B^c(\Lambda)$ . For H-EOS (B), however, the condition  $\mu_\Lambda = \mu_n$  is met at a nonzero value of  $\rho_\Lambda/\rho_B (=0.126)$ , at which  $\mathcal{E}'/\rho_B$  is a local minimum, and the absolute energy minimum still lies at  $\rho_\Lambda/\rho_B = 0$  [Fig. 16(b)]. In this case, the  $\Lambda$  mixing starts at a slightly higher density ( $\sim 0.44 \text{ fm}^{-3}$ ) than  $\rho_B^*(\Lambda)(=0.421 \text{ fm}^{-3})$  with a nonzero value of  $\rho_\Lambda/\rho_B$ .

In both H-EOS (A) and (B), the dependence of the chemical potentials  $\mu_\Lambda$  and  $\mu_n$  on the  $\Lambda$ -mixing ratio is closely correlated to that of the respective baryon potentials  $V_\Lambda$  and  $V_n$ , as seen in Figs. 16(a) and 16(b). In fact, the difference of the onset mechanisms of the  $\Lambda$  mixing between the cases H-EOS (A) and (B) stems from the difference of the dependence of the baryon potentials on the  $\Lambda$ -mixing ratio between H-EOS (A) and (B).

### B. $\Sigma^-$ -mixing

The condition of the  $\Sigma^-$  mixing in the noncondensed  $(n, p, \Lambda, e^-)$  matter is given by Eq. (20c) with  $\theta = 0$ , that is,  $\mu_{\Sigma^-} = \mu_n + \mu$  with

$$\mu_{\Sigma^-} = \frac{(3\pi^2 \rho_{\Sigma^-})^{2/3}}{2M_N} + \delta M_{\Sigma^- N} + V_{\Sigma^-}, \quad (\text{A2})$$

and Eq. (A1b), together with  $\mu_n = \mu_p + \mu$  [Eq. (20a) with  $\theta = 0$ ],  $\mu_\Lambda = \mu_n$  [Eq. (20b) with  $\theta = 0$ ], and the charge neutrality condition,  $\rho_p = \rho_e$ .

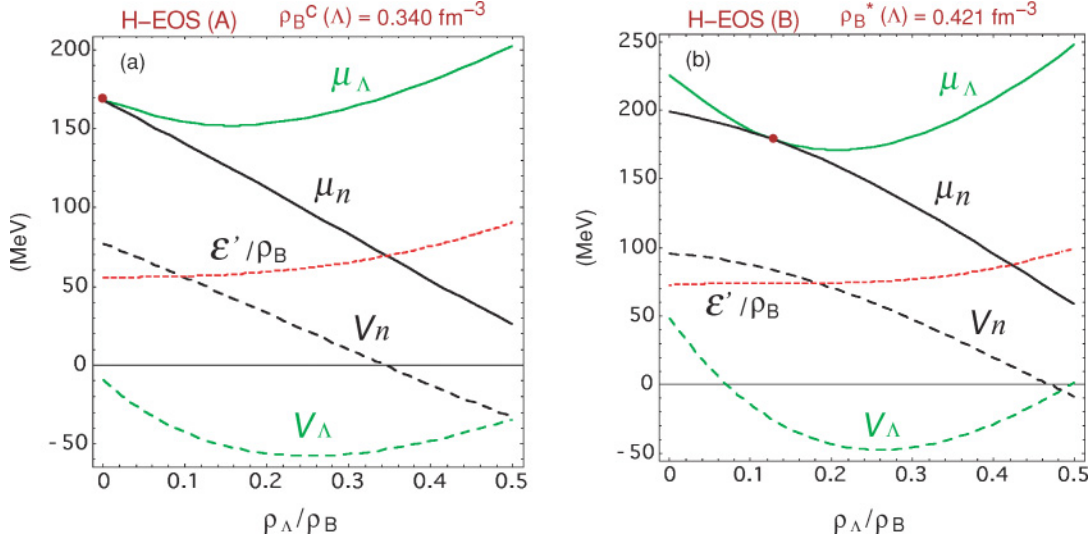


FIG. 16. (Color online) Dependence of  $V_\Lambda$ ,  $V_n$  (dashed lines),  $\mu_\Lambda$ ,  $\mu_n$  (solid lines), and the total energy per baryon  $\mathcal{E}'/\rho_B$  (short dashed line) on the  $\Lambda$ -mixing ratio  $\rho_\Lambda/\rho_B$  in the noncondensed neutron-star matter at the minimal baryon number density  $\rho_B^C(\Lambda)$  above which the  $\Lambda$ -mixing condition,  $\mu_\Lambda = \mu_n$ , is satisfied, for (a) H-EOS (A) and (b) H-EOS (B). See the text for details.

In Fig. 17, we depict the baryon potentials  $V_{\Sigma^-}$  and  $V_n$ , the difference of the  $\Sigma^-$  chemical potential and charge chemical potential ( $\mu_{\Sigma^-} - \mu$ ), the neutron chemical potential  $\mu_n$ , and the total energy per baryon  $\mathcal{E}'/\rho_B$  as functions of the  $\Sigma^-$ -mixing ratio  $\rho_{\Sigma^-}/\rho_B$  in the noncondensed ( $n$ ,  $p$ ,  $\Lambda$ ,  $e^-$ ) matter at the minimal baryon number density  $\rho_B^C(\Sigma^-)$  above which the  $\Sigma^-$ -mixing condition,  $\mu_{\Sigma^-} = \mu_n + \mu$ , is satisfied, for H-EOS (A) and (B). One finds the results on the onset mechanism of the  $\Sigma^-$  mixing similar to the case of the  $\Lambda$  mixing. That is, for H-EOS (A) [Fig. 17(a)], the onset density  $\rho_B^C(\Sigma^-)$  is given by  $\rho_B^C(\Sigma^-) = \rho_B^*(\Sigma^-) (= 0.525 \text{ fm}^{-3})$  with  $\rho_{\Sigma^-}/\rho_B = 0$ ,

and the  $\Sigma^-$ -mixing ratio increases continuously from zero with increase in the baryon number density. For H-EOS (B) [Fig. 17(b)], the onset density  $\rho_B^C(\Sigma^-)$  ( $\sim 0.59 \text{ fm}^{-3}$ ) is slightly larger than the minimal density  $\rho_B^*(\Sigma^-) (= 0.575 \text{ fm}^{-3})$  satisfying the  $\Sigma^-$ -mixing conditions, and the  $\Sigma^-$  mixing starts with a nonzero value of  $\rho_{\Sigma^-}/\rho_B$ . The dependence of the chemical potentials  $\mu_{\Sigma^-}$  and  $\mu_n$  on the  $\Sigma^-$ -mixing ratio is correlated with that of the baryon potentials  $V_{\Sigma^-}$  and  $V_n$ , respectively, which leads to the difference of the onset mechanisms of the  $\Sigma^-$  mixing between H-EOS (A) and (B).

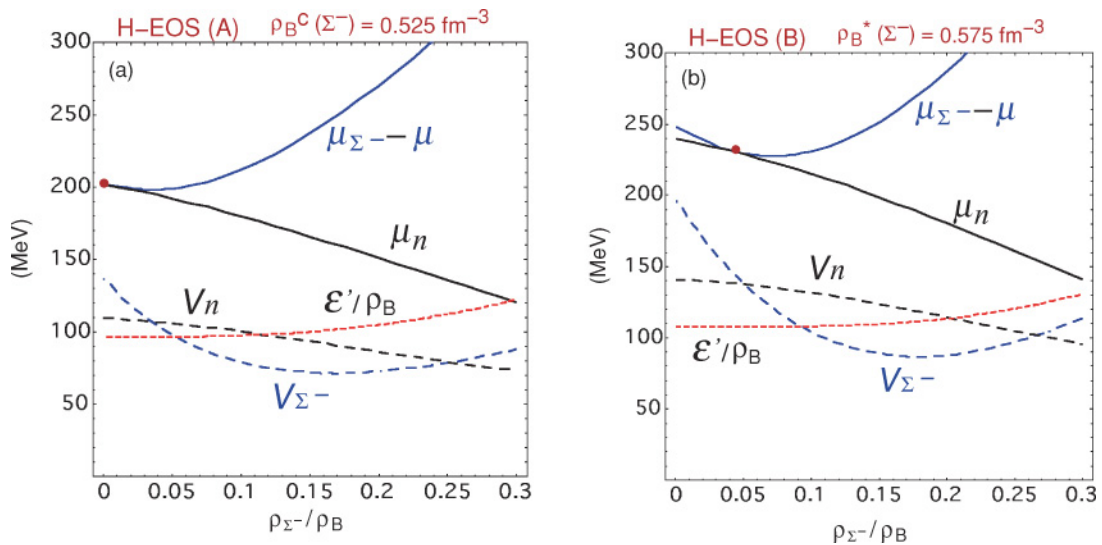


FIG. 17. (Color online) Dependence of the baryon potentials  $V_{\Sigma^-}$ ,  $V_n$  (dashed lines), the difference of the  $\Sigma^-$  chemical potential and charge chemical potential,  $\mu_{\Sigma^-} - \mu$  (solid line), the neutron chemical potential  $\mu_n$  (solid line), and the total energy per baryon  $\mathcal{E}'/\rho_B$  (short dashed line) on the  $\Sigma^-$ -mixing ratio  $\rho_{\Sigma^-}/\rho_B$  in the noncondensed ( $n$ ,  $p$ ,  $\Lambda$ ,  $e^-$ ) matter at the minimal baryon number density  $\rho_B^C(\Sigma^-)$  above which the  $\Sigma^-$ -mixing condition,  $\mu_{\Sigma^-} = \mu_n + \mu$ , is satisfied, for (a) H-EOS (A) and (b) H-EOS (B). See the text for details.



- [1] D. B. Kaplan and A. E. Nelson, Phys. Lett. **B175**, 57 (1986).
- [2] T. Muto, R. Tamagaki, and T. Tatsumi, Prog. Theor. Phys. Suppl. **112**, 159 (1993); T. Muto, T. Takatsuka, R. Tamagaki, and T. Tatsumi, *ibid.* **112**, 221 (1993).
- [3] T. Tatsumi, Prog. Theor. Phys. Suppl. **120**, 111 (1995).
- [4] C.-H. Lee, G. E. Brown, D.-P. Min, and M. Rho, Nucl. Phys. **A585**, 401 (1995).
- [5] H. Fujii, T. Maruyama, T. Muto, and T. Tatsumi, Nucl. Phys. **A597**, 645 (1996).
- [6] C.-H. Lee, Phys. Rep. **275**, 197 (1996).
- [7] M. Prakash, I. Bombaci, M. Prakash, P. J. Ellis, J. M. Lattimer, and R. Knorren, Phys. Rep. **280**, 1 (1997).
- [8] V. Thorsson, M. Prakash, and J. M. Lattimer, Nucl. Phys. **A572**, 693 (1994); **A574**, 851(E) (1994).
- [9] N. K. Glendenning and J. Schaffner-Bielich, Phys. Rev. C **60**, 025803 (1999); N. K. Glendenning, Phys. Rep. **342**, 393 (2001).
- [10] H. Heiselberg, C. J. Pethick, and E. F. Staubo, Phys. Rev. Lett. **70**, 1355 (1993).
- [11] M. B. Christiansen, N. K. Glendenning, and J. Schaffner-Bielich, Phys. Rev. C **62**, 025804 (2000).
- [12] T. Norsen and S. Reddy, Phys. Rev. C **63**, 065804 (2001).
- [13] D. N. Voskresensky, M. Yasuhira, and T. Tatsumi, Nucl. Phys. **A723**, 291 (2003).
- [14] T. Maruyama, T. Tatsumi, D. N. Voskresensky, T. Tanigawa, and S. Chiba, Nucl. Phys. **A749**, 186c (2005); T. Maruyama, T. Tatsumi, D. N. Voskresensky, T. Tanigawa, T. Endo, and S. Chiba, Phys. Rev. C **73**, 035802 (2006); T. Maruyama, T. Tatsumi, T. Endo, and S. Chiba, Recent Res. Devel. Physics **7**, 1 (2006).
- [15] G. E. Brown and H. A. Bethe, Astrophys. J. **423**, 659 (1994).
- [16] T. W. Baumgarte, S. L. Shapiro, and S. Teukolsky, Astrophys. J. **443**, 717 (1995); **458**, 680 (1996).
- [17] J. A. Pons, S. Reddy, P. J. Ellis, M. Prakash, and J. M. Lattimer, Phys. Rev. C **62**, 035803 (2000); Astrophys. J. **553**, 382 (2001).
- [18] T. Tatsumi and M. Yasuhira, Nucl. Phys. **A653**, 133 (1999); M. Yasuhira and T. Tatsumi, *ibid.* **A690**, 769 (2001).
- [19] G. E. Brown, K. Kubodera, D. Page, and P. Pizzocherri, Phys. Rev. D **37**, 2042 (1988).
- [20] T. Tatsumi, Prog. Theor. Phys. **80**, 22 (1988).
- [21] D. Page and E. Baron, Astrophys. J. **354**, L17 (1990).
- [22] H. Fujii, T. Muto, T. Tatsumi, and R. Tamagaki, Nucl. Phys. **A571**, 758 (1994); Phys. Rev. C **50**, 3140 (1994).
- [23] T. Muto and T. Tatsumi, Phys. Lett. **B283**, 165 (1992).
- [24] G. E. Brown, K. Kubodera, M. Rho, and V. Thorsson, Phys. Lett. **B291**, 355 (1992).
- [25] T. Muto, Prog. Theor. Phys. **89**, 415 (1993).
- [26] E. E. Kolomeitsev, D. N. Voskresensky, and B. Kämpfer, Nucl. Phys. **A588**, 889 (1995).
- [27] N. K. Glendenning, Astrophys. J. **293**, 470 (1985); N. K. Glendenning and S. A. Moszkowski, Phys. Rev. Lett. **67**, 2414 (1991).
- [28] P. J. Ellis, R. Knorren, and M. Prakash, Phys. Lett. **B349**, 11 (1995); R. Knorren, M. Prakash, and P. J. Ellis, Phys. Rev. C **52**, 3470 (1995).
- [29] J. Schaffner and I. N. Mishustin, Phys. Rev. C **53**, 1416 (1996).
- [30] S. Pal, M. Hanauske, I. Zakout, H. Stöcker, and W. Greiner, Phys. Rev. C **60**, 015802 (1999).
- [31] M. Hanauske, D. Zschesche, S. Pal, S. Schramm, H. Stöcker, and W. Greiner, Astrophys. J. **537**, 958 (2000).
- [32] P. K. Sahu, Phys. Rev. C **62**, 045801 (2000).
- [33] H. Huber, F. Weber, M. K. Weigel, and Ch. Schaab, Int. J. Mod. Phys. E **7**, 301 (1998).
- [34] M. Baldo, G. F. Burgio, and H.-J. Schulze, Phys. Rev. C **58**, 3688 (1998); **61**, 055801 (2000).
- [35] I. Vidaña, A. Polls, A. Ramos, M. Hjorth-Jensen, and V. G. J. Stoks, Phys. Rev. C **61**, 025802 (2000); I. Vidaña, A. Polls, A. Ramos, L. Engvik, and M. Hjorth-Jensen, *ibid.* **62**, 035801 (2000).
- [36] S. Balberg and A. Gal, Nucl. Phys. **A625**, 435 (1997).
- [37] S. Nishizaki, Y. Yamamoto, and T. Takatsuka, Prog. Theor. Phys. **108**, 703 (2002).
- [38] T. Takatsuka, Prog. Theor. Phys. Suppl. **156**, 84 (2004).
- [39] S. Pal, D. Bandyopadhyay, and W. Greiner, Nucl. Phys. **A674**, 553 (2000).
- [40] S. Banik and D. Bandyopadhyay, Phys. Rev. C **63**, 035802 (2001); **64**, 055805 (2001).
- [41] D. P. Menezes, P. K. Panda, and C. Providencia, Phys. Rev. C **72**, 035802 (2005).
- [42] C. Y. Ryu, C. H. Hyun, S. W. Hong, and B. T. Kim, Phys. Rev. C **75**, 055804 (2007).
- [43] T. Muto, Nucl. Phys. **A691**, 447c (2001); **A697**, 225 (2002).
- [44] E. E. Kolomeitsev and D. N. Voskresensky, Phys. Rev. C **68**, 015803 (2003).
- [45] A. Gal, Prog. Theor. Phys. Suppl. **156**, 1 (2004), and references therein.
- [46] T. Muto (unpublished).
- [47] K. Tsushima, K. Saito, A. W. Thomas, and S. V. Wright, Phys. Lett. **B429**, 239 (1998); **B436**, 453 (1998) (E).
- [48] S. J. Dong, J.-F. Lagaë, and K. F. Liu, Phys. Rev. D **54**, 5496 (1996).
- [49] D. J. Millener, C. B. Dover, and A. Gal, Phys. Rev. C **38**, 2700 (1988).
- [50] M. Kohno, Y. Fujiwara, T. Fujita, C. Nakamoto, and Y. Suzuki, Nucl. Phys. **A674**, 229 (2000).
- [51] Y. Fujiwara, M. Kohno, C. Nakamoto, and Y. Suzuki, Phys. Rev. C **64**, 054001 (2001).
- [52] S. Bart *et al.*, Phys. Rev. Lett. **83**, 5238 (1999).
- [53] J. Dabrowski, Phys. Rev. C **60**, 025205 (1999).
- [54] H. Noumi *et al.*, Phys. Rev. Lett. **89**, 072301 (2002); **90**, 049902(E) (2003).
- [55] J. Dabrowski and J. Rozynek, Acta Phys. Polon. B **35**, 2303 (2004).
- [56] T. Harada and Y. Hirabayashi, Nucl. Phys. **A759**, 143 (2005).
- [57] J. Mares, E. Friedman, A. Gal, and B. K. Jennings, Nucl. Phys. **A594**, 311 (1995).
- [58] J. P. Blaizot, Phys. Rep. **64**, 171 (1980).
- [59] T. Muto, Nucl. Phys. **A754**, 350c (2005); T. Muto, AIP Conf. Proc. **847**, 439 (2006).
- [60] N. Itoh, Prog. Theor. Phys. **44**, 291 (1970).
- [61] A. R. Bodmer, Phys. Rev. D **4**, 1601 (1971).
- [62] S. A. Chin and A. K. Kerman, Phys. Rev. Lett. **43**, 1292 (1979).
- [63] E. Witten, Phys. Rev. D **30**, 272 (1984).
- [64] E. Farhi and R. L. Jaffe, Phys. Rev. D **30**, 2379 (1984).
- [65] T. D. Lee and G. C. Wick, Phys. Rev. D **9**, 2291 (1974).
- [66] J. B. Hartle *et al.*, Astrophys. J. **199**, 471 (1975).
- [67] A. B. Migdal *et al.*, Phys. Lett. **B65**, 423 (1976).
- [68] B. W. Lynn, A. E. Nelson, and N. Tetradis, Nucl. Phys. **B345**, 186 (1990).
- [69] J. Schaffner-Bielich, M. Hanauske, H. Stöcker, and W. Greiner, Phys. Rev. Lett. **89**, 171101 (2002).

- [70] Y. Akaishi and T. Yamazaki, Phys. Rev. C **65**, 044005 (2002); T. Yamazaki and Y. Akaishi, Phys. Lett. **B535**, 70 (2002).
- [71] A. Dote, H. Horiuchi, Y. Akaishi, and T. Yamazaki, Phys. Lett. **B590**, 51 (2004); Phys. Rev. C **70**, 044313 (2004).
- [72] T. Yamazaki, A. Dote, and Y. Akaishi, Phys. Lett. **B587**, 167 (2004).
- [73] T. Kishimoto, Phys. Rev. Lett. **83**, 4701 (1999).
- [74] M. Iwasaki *et al.*, Nucl. Instrum. Methods Phys. Res., Sect. A **473**, 286 (2001).
- [75] T. Kishimoto *et al.*, Prog. Theor. Phys. Suppl. **149**, 264 (2003); Nucl. Phys. **A754**, 383c (2005).
- [76] M. Iwasaki *et al.*, nucl-ex/0310018; T. Suzuki *et al.*, Nucl. Phys. **A754**, 375c (2005); Phys. Lett. **B597**, 263 (2004).
- [77] M. Agnello *et al.*, Phys. Rev. Lett. **94**, 212303 (2005).
- [78] J. Mareš, E. Friedman, and A. Gal, Phys. Lett. **B606**, 295 (2005); Nucl. Phys. **A770**, 84 (2006).
- [79] J. Yamagata, H. Nagahiro, Y. Okumura, and S. Hirenzaki, Prog. Theor. Phys. **114**, 301 (2005); **114**, 905(E) (2005); J. Yamagata, H. Nagahiro, and S. Hirenzaki, Phys. Rev. C **74**, 014604 (2006).
- [80] E. Oset and H. Toki, Phys. Rev. C **74**, 015207 (2006); V. K. Magas, E. Oset, A. Ramos, and H. Toki, Phys. Rev. C **74**, 025206 (2006).
- [81] For a review, see A. Nakamura, T. Hatsuda, A. Hosaka, and T. Kunihiro, Prog. Theor. Phys. Suppl. **153**, 1 (2004).
- [82] P. F. Bedaque and T. Schäfer, Nucl. Phys. **A697**, 802 (2002).
- [83] D. B. Kaplan and S. Reddy, Phys. Rev. D **65**, 054042 (2002).
- [84] M. Buballa, Phys. Lett. **B609**, 57 (2005).
- [85] Michael McNeil Forbes, Phys. Rev. D **72**, 094032 (2005).
- [86] S. Banik and D. Bandyopadhyay, Phys. Rev. D **67**, 123003 (2003).